

AD 607442

# Separated Flow Past Slender Delta Wings with Secondary Vortex Simulation

24 AUGUST 1964

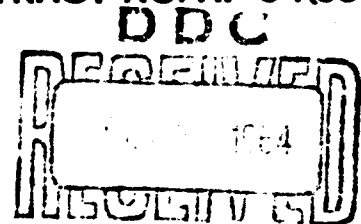
Prepared by  
BERNARD PERSHING

Prepared for COMMANDER SPACE SYSTEMS DIVISION  
AIR FORCE SYSTEMS COMMAND  
LOS ANGELES AIR FORCE STATION  
*Los Angeles, California*

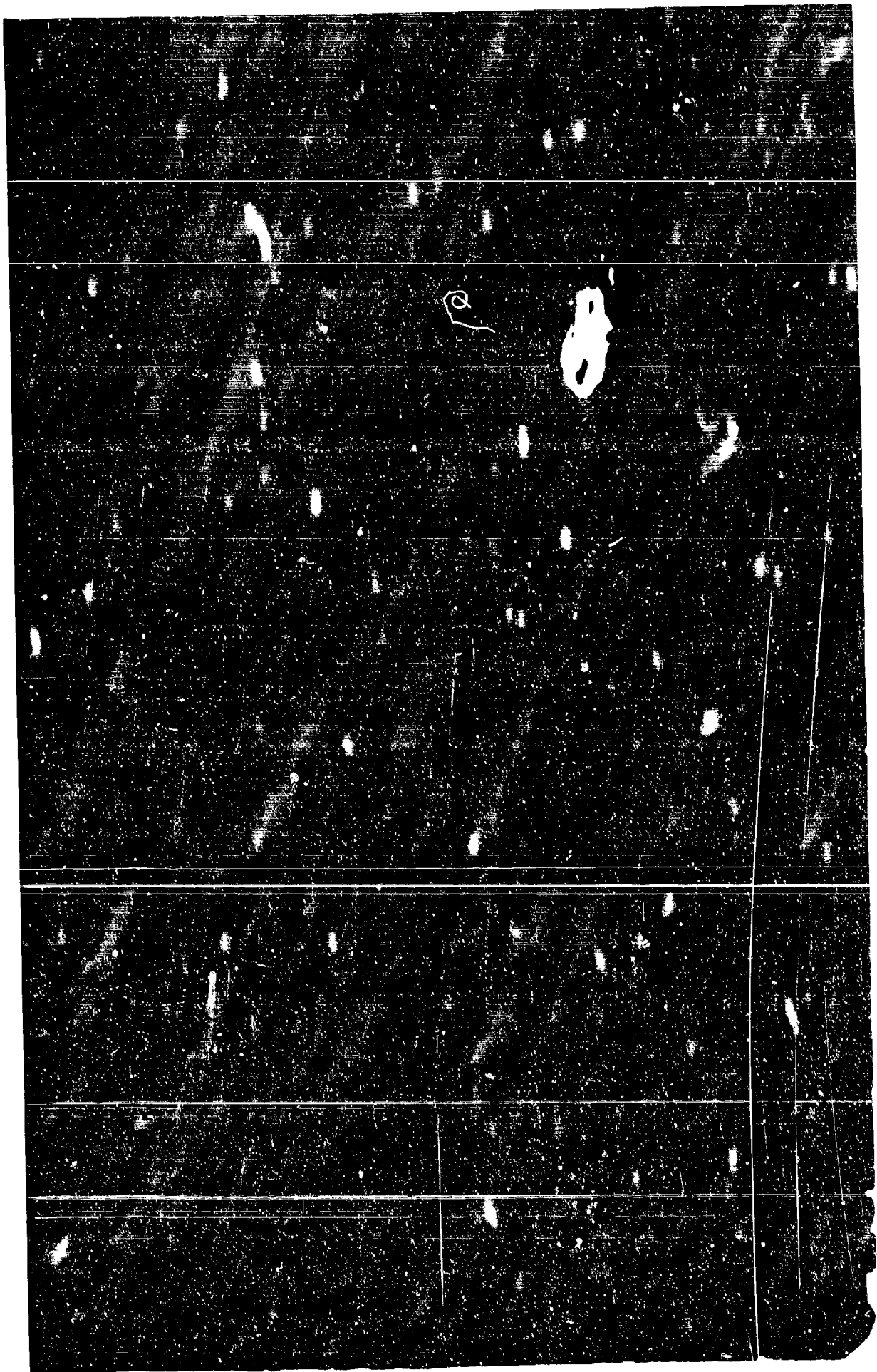
COPY <u>2</u> OF <u>3</u> <i>mg</i>	
HARD COPY	\$ .300
MICROFICHE	\$ .075



EL SEGUNDO TECHNICAL OPERATIONS • AEROSPACE CORPORATION  
CONTRACT NO. AF 04(695)-269



DDC IRA D



SEPARATED FLOW PAST SLENDER DELTA WINGS  
WITH SECONDARY VORTEX SIMULATION

Prepared by  
Bernard Pershing

El Segundo Technical Operations  
AEROSPACE CORPORATION  
El Segundo, California

Contract No. AF 04(695)-269

24 August 1964

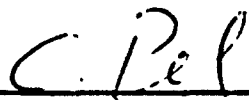
Prepared for  
COMMANDER SPACE SYSTEMS DIVISION  
AIR FORCE SYSTEMS COMMAND  
LOS ANGELES AIR FORCE STATION  
Los Angeles, California

SEPARATED FLOW PAST SLENDER DELTA WING<sup>o</sup>  
WITH SECONDARY VORTEX SIMULATION

Prepared by

  
Bernard Pershing

Approved by

  
C. Pel, Associate Head  
Fluid Mechanics Department

  
W. F. Radcliffe, Director  
Engineering Sciences Subdivision  
Applied Mechanics Division

This technical documentary report has been reviewed and is approved for publication and dissemination. The conclusions and findings contained herein do not necessarily represent an official Air Force position.

For Space Systems Division  
Air Force Systems Command

  
David Kauffman  
1st Lt, USAF

## ABSTRACT

The flow about a slender flat-plate delta wing at angle-of-attack is represented by replacing the vortex core-feeding sheet system associated with leading edge separation by a force-free concentrated vortex. Secondary flow phenomena near the leading edge are approximated by allowing infinite flow velocity around the leading edge. The problem is reduced to a two-dimensional one by assuming a conical field and using slender wing theory.

Computed pressure and lift distribution, vortex position, lift coefficient, and flow patterns are compared with test data and with the theories of Brown and Michael, and Mangler and Smith. The nonlinear characteristics of the lift curve with angle-of-attack and the strong influence of secondary flow simulation on vortex position and pressure distribution are displayed. The vortex is shown to be further inboard than predicted by previous theories and to correlate well with experiment. The nonlinear component of lift, the pressure distribution, and surface flow pattern are also shown to correlate well with experiment.

## CONTENTS

ABSTRACT .....	
NOMENCLATURE .....	xi
I. INTRODUCTION .....	1
II. ANALYSIS .....	5
A. Basic Model .....	5
B. Boundary Conditions .....	7
C. Potential Solution .....	11
D. Calculation of the Force on the Wing .....	19
E. Pressure Distribution and Span Loading .....	23
F. Streamlines and Stagnation Points .....	28
III. DISCUSSION OF RESULTS .....	37
IV. CONCLUSIONS .....	43
APPENDIX .....	45
REFERENCES .....	47

## ILLUSTRATIONS

1.	The Characteristics of the Flow Field About a Slender Flat-Plate Delta Wing . . . . .	2
2.	Coordinate System . . . . .	6
3.	Schematic Diagram of the Separated Flow Around Wing Leading Edge . . . . .	10
4.	Generation of the Concentrated Vortex . . . . .	12
5.	Transformed Coordinate Systems . . . . .	13
6.	Computed Vortex Location . . . . .	17
7.	Comparison of Calculated and Measured Vortex Lateral Position . . . . .	18
8.	Variation of Vortex Strength with Angle-of-Attack . . . . .	20
9.	Calculated Lift Coefficient . . . . .	21
10.	Comparison of Computed and Measured Nonlinear Component of Lift Coefficient . . . . .	24
11.	Comparison of Calculated and Measured Pressure Coefficient . . . . .	27
12.	Comparison of Computed and Measured Span Loadings . . . . .	29
13.	Streamline Defined in $\theta$ Plane . . . . .	31
14.	Streamline Patterns in the Cross-Flow Plane . . . . .	32
15.	Stagnation Line Location . . . . .	33
16.	Computed Surface Streamlines on a $20^\circ$ Delta Wing . . . . .	35
17.	Drag Coefficient of a Two Dimensional Wedge . . . . .	39
18.	Flow in the Plane Perpendicular to the Leading Edge . . . . .	40
19.	Force-Free Vortex Position and Strength . . . . .	46

## NOMENCLATURE

a	semi-span at chordwise station x
AR	aspect ratio
$C_L$	lift coefficient, $\frac{L}{\frac{1}{2} \rho U^2 S}$
$C_{L_\alpha}$	lift curve slope
$C_P$	pressure, coefficient, $\frac{P_{\text{local}} - P_{\text{free stream}}}{\frac{1}{2} \rho U^2}$
k	vortex-core strength
M	Mach number
p	pressure
q	magnitude of cross-flow velocity vector
r	magnitude of $\zeta$ , $\sqrt{Y^2 + Z^2}$
S	wing area
t	time
U	free-stream velocity
v,w	disturbance velocity in y and z direction, respectively
W	complex velocity potential, $\Phi + i\psi$
x	coordinate along wing in free stream direction
y	coordinate along wing normal to free stream
Y	real part of $\zeta$
z	coordinate normal to wing surface
Z	imaginary part of $\zeta$
$\alpha$	angle-of-attack

## NOMENCLATURE (Continued)

$\beta$	argument of $\zeta$ , $\tan^{-1} \frac{Z}{Y}$
$\epsilon$	semi-apex angle of delta wing
$\zeta$	vector distance in circle plane, $\zeta = Y + iZ$ (see Fig. 5)
$\eta$	imaginary part of $\theta$
$\theta$	vector distance in $\theta$ plane, $\theta = \xi + i\eta$ (see Fig. 5)
$\xi$	real part of $\theta$
$\rho$	density
$\sigma$	vector distance in physical cross-flow plane, $x + iy$ (see Fig. 5)
$\Phi$	disturbance velocity potential - real part of $W$
$\Psi$	stream function - imaginary part of $W$
$(\bar{\quad})$	complex conjugate of quantity ( $\quad$ )

### Subscripts

$o$	value at vortex position
$\infty$	free stream condition

### Superscripts

*	condition with the right vortex removed
---	-----------------------------------------

## I. INTRODUCTION

In recent years, the concentrated effort on high speed research has overshadowed the low speed problem areas associated with low aspect ratio wings and slender lifting bodies. With the advent of actual "hardware" there has been a forced return to the consideration of low speed slender wing theory. Particular interest has been directed toward the case of delta wings with leading edge flow separation. This class of flows has been investigated experimentally and analytically, but theoretical efforts to predict the basic aerodynamic characteristics have been only partially successful.

The principle features of separated flow about thin delta wings are presented in Fig. 1. The separated flow shed from the leading edges form conical spirals which curl up over the top of the wing into cores of concentrated vorticity. These cores and their generating sheets are the primary vortex system. Large negative pressure peaks and strong adverse pressure gradients outboard of the peaks are produced on the wing upper surface. The boundary layer separates in the area of the adverse pressure gradient and forms a secondary vortex system which, by virtue of its proximity to the wing surface and leading edge, has a significant effect on the pressure distribution and the strength and position of the primary vortex system. The exact nature of the secondary vortex system is not well understood and, in fact, several flow visualization studies (Refs. 1 and 2) indicate that for certain conditions, it may consist of two or more sets of vortices generated by the boundary layer.

Previous analyses (Refs. 3, 4, and 5) of this problem have replaced the primary vortex system with an equivalent set of symmetrically located concentrated vortices above the wing. Conical flow is assumed and slender body techniques are used to determine the vortex strength and position through application of suitable boundary conditions. Legendre (Ref. 3) requires a force-free vortex and application of the Kutta condition at the wing leading edge. No attempt is made to account for the effect of the vortex

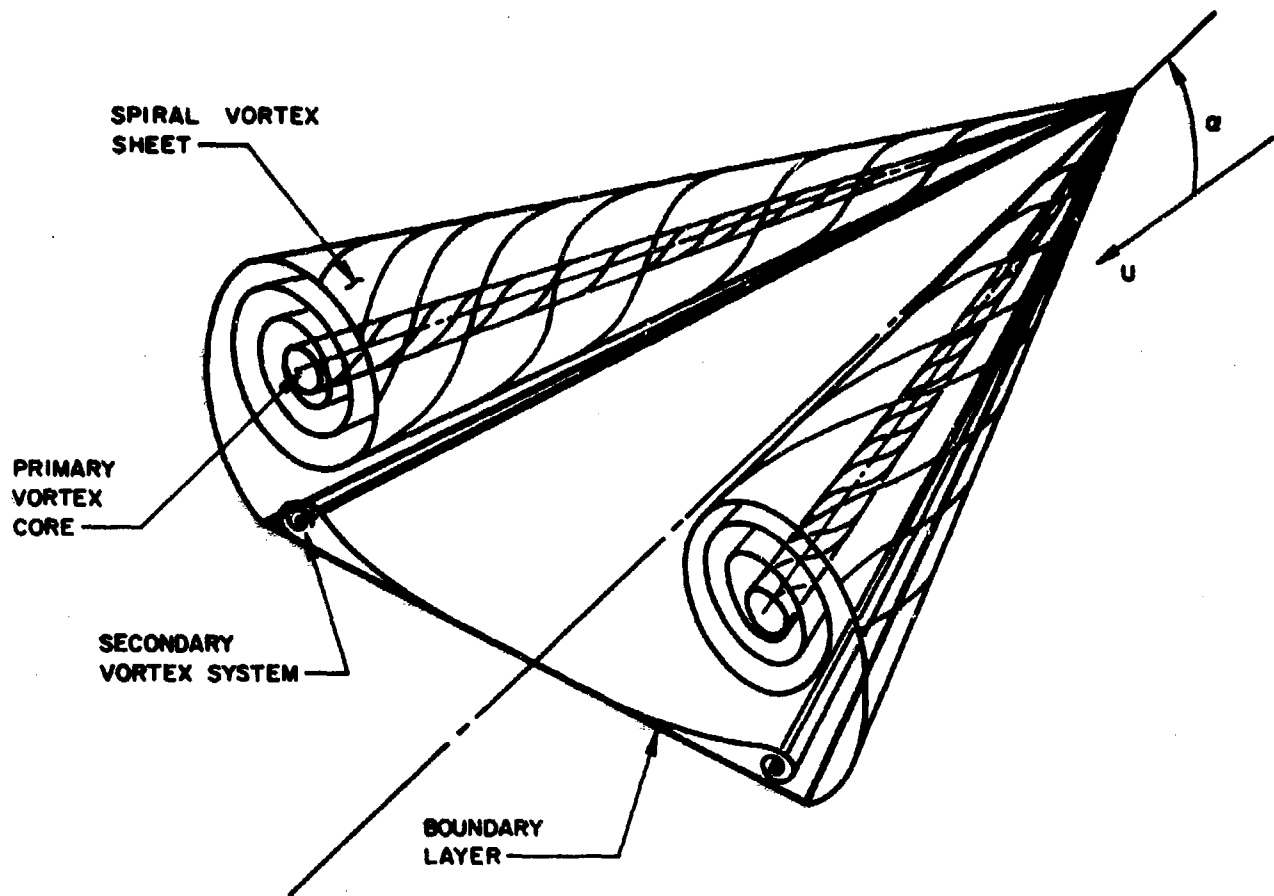


Figure 1. The Characteristics of the Flow Field About a Slender Flat-Plate Delta Wing.

feeding sheet and, as a result, the isolated vortices, whose strength increases with streamwise coordinate violate Kelvin's theorem of the constancy of circulation. This results in a multi-valued solution to the wing force system (Refs. 6 and 7). Brown and Michael (Ref. 4) attempt to eliminate the multi-valued character of the force system by postulating concentrated vortices fed by planar feeding sheets; the vortices and feeding sheets each sustain balancing forces such that the net force on the system is zero. The models of Legendre, and Brown and Michael, have been only partially satisfactory in predicting vortex position, lift coefficient, and pressure distribution. Subsequent analyses (Ref. 5) have incorporated refinements in the primary vortex feeding sheet structure with only minor improvement in results.

The discrepancy between theory and experiment is generally attributed to the presence of the secondary vortex system which has not been considered in previous analysis. Because of its proximity to the wing surface, the secondary flow is believed to influence the solution to a large extent. The secondary vortex system has been mentioned by Brown and Michael, and Mangler and Smith; a very interesting discussion of the problem is given by Rott (Ref. 8) wherein it is pointed out that due to secondary flow the application of the Kutta condition for a single vortex model makes no sense and at most, only semi-empirical results could be expected.

It is apparent that for improved results the secondary vortex system must be taken into account. The solution of the problem, considering both vortex systems, is beyond present capability.

An approximation of the real flow must be resorted to which will possess the characteristics of the primary and secondary vortex systems and will not require the solution of the complete equations of fluid flow with viscous dissipation.

The present analysis attempts to account for the effects of secondary vortex formation using a simple model. The secondary vortex system is simulated by an appropriate modification of the boundary conditions. A flat-plate delta wing is considered and, as in the previous analyses, conical flow is assumed and slender body techniques are applied to obtain solutions in the cross-flow plane.

## II. ANALYSIS

### A. BASIC MODEL

The flow about a slender flat-plate delta wing placed at an angle-of-attack to the free stream is considered. The aspect ratio is restricted to small values so that conical flow may be assumed. The physical flow, as represented in Fig. 1, is dominated by sheets of vorticity which emanate from the leading edges and roll up into spirals over the wing upper surface to form the well-defined primary vortex cores. The vortex cores induce strong negative pressure peaks on the wing upper surface and large adverse pressure gradients outboard of the peaks. Boundary layer separation occurs in this area and secondary vortices are formed which lie close to the wing surface. The strength of the vorticity emanating from the leading edge is a function of the direction and magnitude of that component of the free stream velocity which is perpendicular to the leading edge. For a given wing semi-vertex angle  $\epsilon$  and angle-of-attack  $\alpha$ , the vorticity emanates at a constant rate along the leading edge and feeds into the primary vortex core causing it to grow linearly with streamwise coordinate.

The solution of this type of flow is made tractable by replacing the primary vortex sheet-core system with a pair of concentrated vortices located at the center of the feeding sheet spirals. This representation preserves the general characteristics of the real flow. The coordinate system employed is shown in Fig. 2. The origin is located at the apex of the delta planform, the  $x$  axis is directed downstream and coincides with the wing centerline, the  $y$  axis is horizontal and positive to the right as viewed upstream, and the  $z$  axis is perpendicular to the wing plane, positive up. The equation of motion to be satisfied for the slightly disturbed flow of the inviscid fluid is the Prandtl-Glauert differential equation

$$(1 - M^2)\phi_{xx} + \phi_{yy} + \phi_{zz} = 0 \quad (1)$$

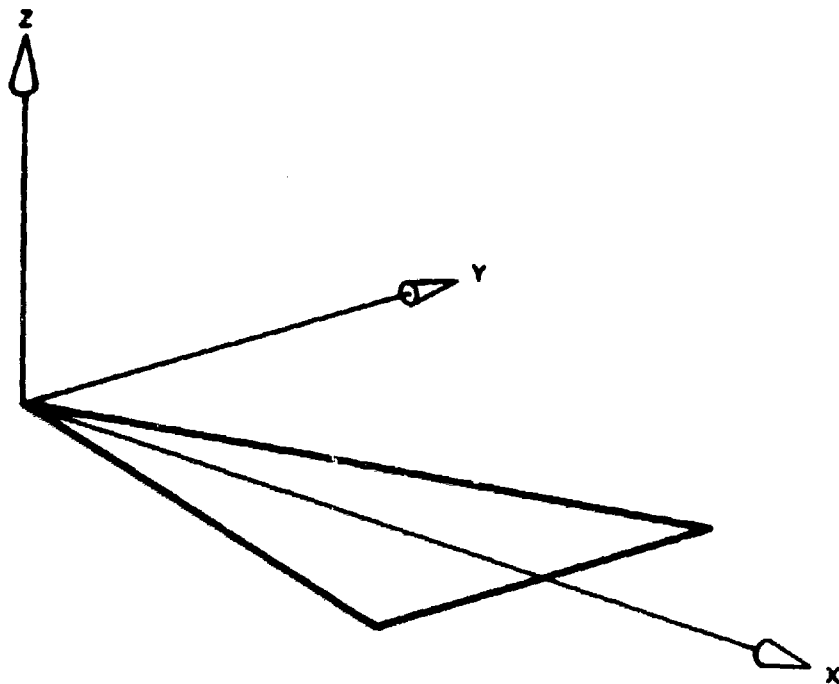


Figure 2. Coordinate System.

where  $\Phi$  is the perturbation velocity potential and  $M$  is the free stream Mach number. Employing the restriction of low aspect ratio planform and Mach number of order 1, the term  $(1 - M^2)\Phi_{xx}$  is neglected and the equation of motion becomes

$$\Phi_{yy} + \Phi_{zz} = 0 \quad (2)$$

Equation (2) is the two-dimensional Laplace equation in the  $y$ - $z$  cross-flow plane and allows the use of slender body theory techniques.

## B. BOUNDARY CONDITIONS

The boundary conditions applied to the present model are the same as those of Legendre except that the Kutta condition at the leading edge is replaced by requiring the ratio between  $\alpha$  and the vortex-wing plane angle to be invariant. The Legendre model is somewhat unsatisfactory because of its inaccurate representation of the vortex feeding sheet structure. However, it is employed here because the potentially more satisfactory Brown and Michael model yields negative results when the Kutta condition is relinquished. Alternate models, primarily those of multi-vortex structure, are far more complex; they are considered to represent a refinement and/or correction to the basic ideas of the present analysis rather than a starting point. Use of the Legendre model must therefore be recognized as an attempt to examine the basic characteristics of secondary flow with the simplest technique available. These points are discussed in further detail in the appendix.

The boundary conditions applied to the present model are: (1) at the wing surface, the normal component of velocity must vanish; (2) at infinity, the perturbation velocity must vanish; (3) the concentrated vortices lie on streamlines; and (4) the concentrated vortices form an angle of  $\alpha/4$  with the wing plane. Conditions (3) and (4) allow determination of the vortex location and strength in the  $y$ - $z$  cross-flow plane.

With the  $y$ - $z$  plane fixed in space and the delta wing passing through it at free stream velocity  $U$ , the flow can be considered two-dimensional and unsteady, the variation with time  $t$  being obtained from the relationship  $x = Ut$  and the condition of conical flow. The vortices will lie on a streamline if the sum of the steady-state and time-dependent components of velocity at the vortex location is equal to zero. The local wing semi-span is  $a(t)$  and the vortex location is given by the vector  $\sigma_o(t) = y_o + iz_o$ . For a fixed angle of attack  $\alpha$  and semi-vertex angle  $\epsilon$ , the quantity  $\sigma_o(t)/a(t)$  is constant by virtue of conical symmetry. We then have

$$\sigma_o(t) = (\sigma_o/a)a(t) \quad (3)$$

The growth rate of  $\sigma_o$  with respect to time is

$$\frac{d\sigma_o}{dt} = (\sigma_o/a) \frac{da}{dt} \quad (4)$$

With respect to an observer at  $\sigma_o$ , this represents a fluid velocity  $-d\sigma_o/dt$ . Substituting  $U\epsilon$  for  $da/dt$ , we obtain, for the time-dependent component of velocity,

$$\frac{d\sigma_o}{dt} = -(\sigma_o/a)U\epsilon \quad (5)$$

The steady-state two-dimensional perturbation velocity at  $\sigma_o$  is  $(v_o + iw_o)^*$ . The superscript  $*$  denotes the velocity obtained by forming the expression for the perturbation velocity minus the velocity due to the vortex at  $\sigma_o$  and taking the limit as  $\sigma$  approaches  $\sigma_o$ . The boundary condition on the vortex is then

$$(v_o + iw_o)^* - (\sigma_o/a)U\epsilon = 0 \quad (6)$$

The real and imaginary parts of Eq. (6) yield two algebraic expressions; one more is required to define the vortex system. Previously, this has been the stipulation that the flow leave the leading edge tangentially. This condition is obtained by requiring the velocity at the leading edge to be bounded. Rather than this boundary condition, the present analysis assumes that the vortices form a fixed angle of  $\alpha/4$  with the wing plane. Consequently, the Kutta condition is not satisfied at the leading edge. The flow from the bottom of the wing turns around the leading edge and travels inboard on the upper surface for a short distance until its velocity reduces to zero and an outboard stagnation point is formed. As a result, a flow singularity exists at the leading edge, as in the slender wing theory of Jones (Ref. 9); in fact, the Jones solution is the first order approximation in  $\alpha$  to the higher order solution obtained herein.

The existence of the outboard stagnation point is critical to this analysis because it introduces the effects of the boundary layer-induced secondary vortex system into the model. This is illustrated by the simplified flow patterns in Fig. 3. An idealized model of the flow with the Kutta condition applied at the leading edge is shown in Fig. 3a. The flow leaves the bottom surface of the wing smoothly and the streamline emanating from the wing tip encircles the vortex L and reattaches to the upper surface near the wing centerline. The fluid confined by the wing and stagnation streamline rotates counterclockwise under the influence of L. The upper surface experiences a large negative pressure peak and adverse spanwise pressure gradient which, in the real flow, induces a boundary layer separation. The real flow is represented schematically in Fig. 3b with the secondary vortex system denoted by M. The flow field induced by M is clockwise. Near the wing tip and close to the surface, M is dominant because of its proximity, and the flow is directed inboard. Further inboard, however, L is dominant and the flow is directed outboard. At some spanwise location B intermediate to L and M, a stagnation point exists, and the streamline emanating from B passes between L and M. This flow can be reproduced by the introduction of the outboard stagnation point as shown in Fig. 3c, and it is seen that although

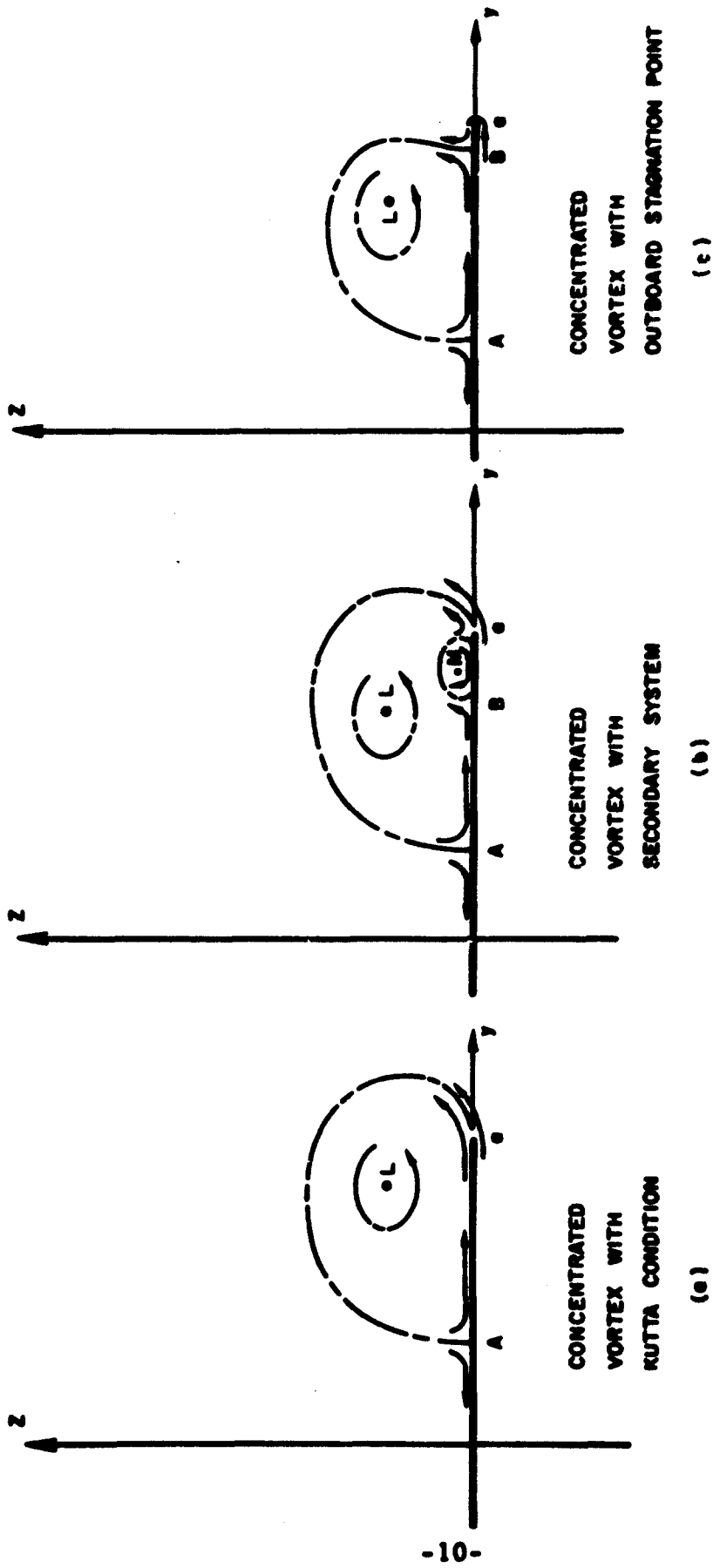


Figure 3. Schematic Diagram of the Separated Flow Around Wing Leading Edge.

the secondary vortex is not explicitly displayed in the velocity potential describing the flow model, its primary effects are present at the surface of the wing.

The stipulation that the concentrated vortices form an angle of  $\alpha/4$  with the wing plane is based on the model shown in Fig. 4. Each element of the leading edge generates vorticity at a constant rate. The vorticity is carried downstream at the angle of local flow and rolls up into the core depicted in Fig. 1. The sheet can be represented by a number of finite filaments originating at uniformly spaced points along the leading edge. The angle between the filaments and the wing plane is  $\alpha/2$  for the limiting case of vanishing aspect ratio (Ref. 10). This value has also been used with success by Gersten (Ref. 11) for slender wings of nonvanishing aspect ratio. The net effect of the filament series is considered to be the same as that of a single vortex with strength equal to the sum of the filaments and located at their center of gravity. The equivalent concentrated vortex therefore forms an angle of  $\alpha/4$  with the wing plane.

### C. POTENTIAL SOLUTION

The complex perturbation velocity potential  $W(\sigma)$  is sought which is a solution of Eq. (2) and fulfills the specified boundary conditions. The flow in the  $y$ - $z$  plane is considered two-dimensional and unsteady with the time dependence entering through the relationship

$$a = \epsilon x = \epsilon U t \quad (7)$$

The analysis is performed in one of three planes (see Fig. 5). In the physical or  $\sigma$  plane, the wing surface lies on the real axis with leading edges at  $\pm a$ . The vector distance is

$$\sigma = y + iz \quad (8)$$

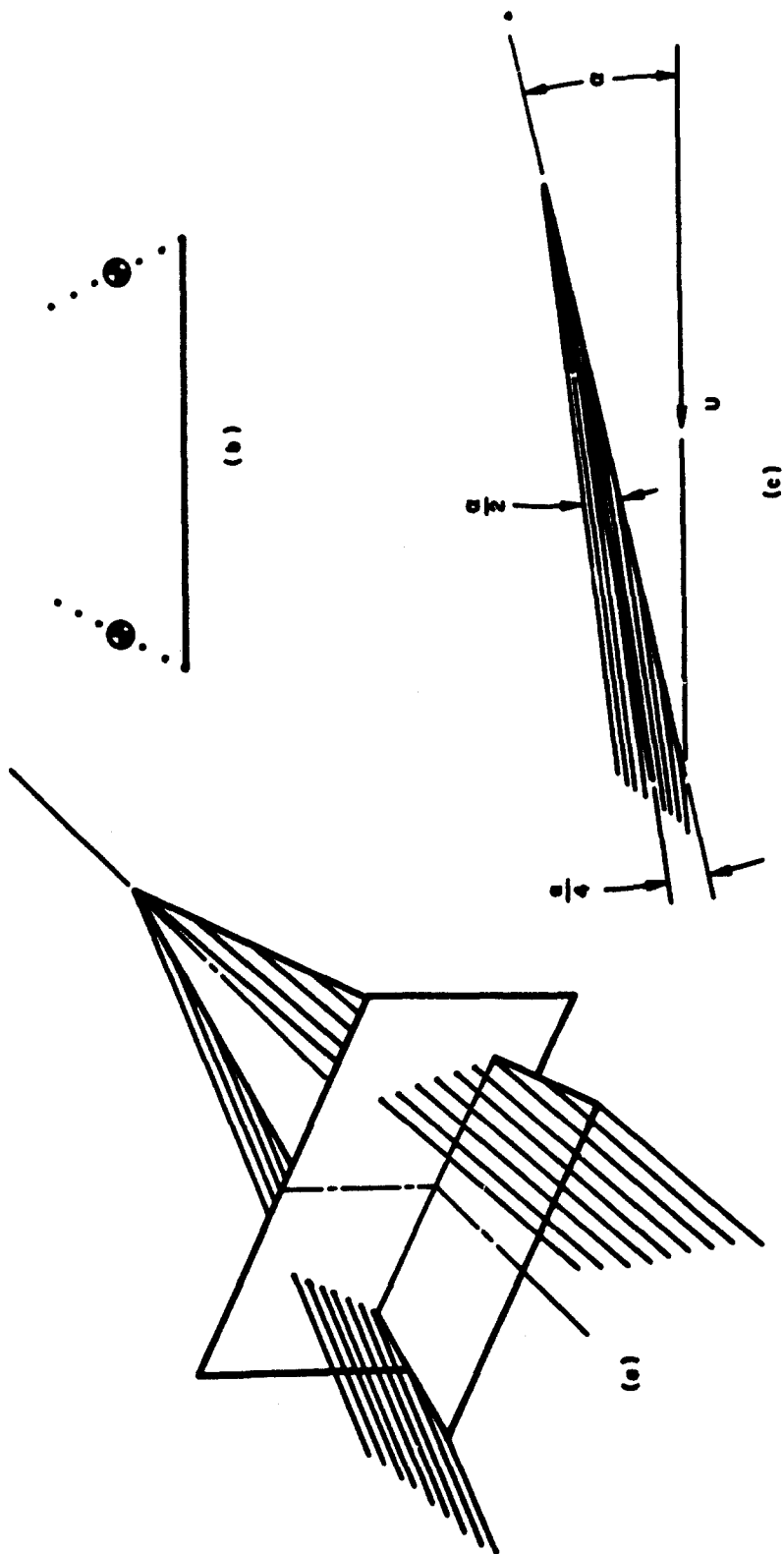
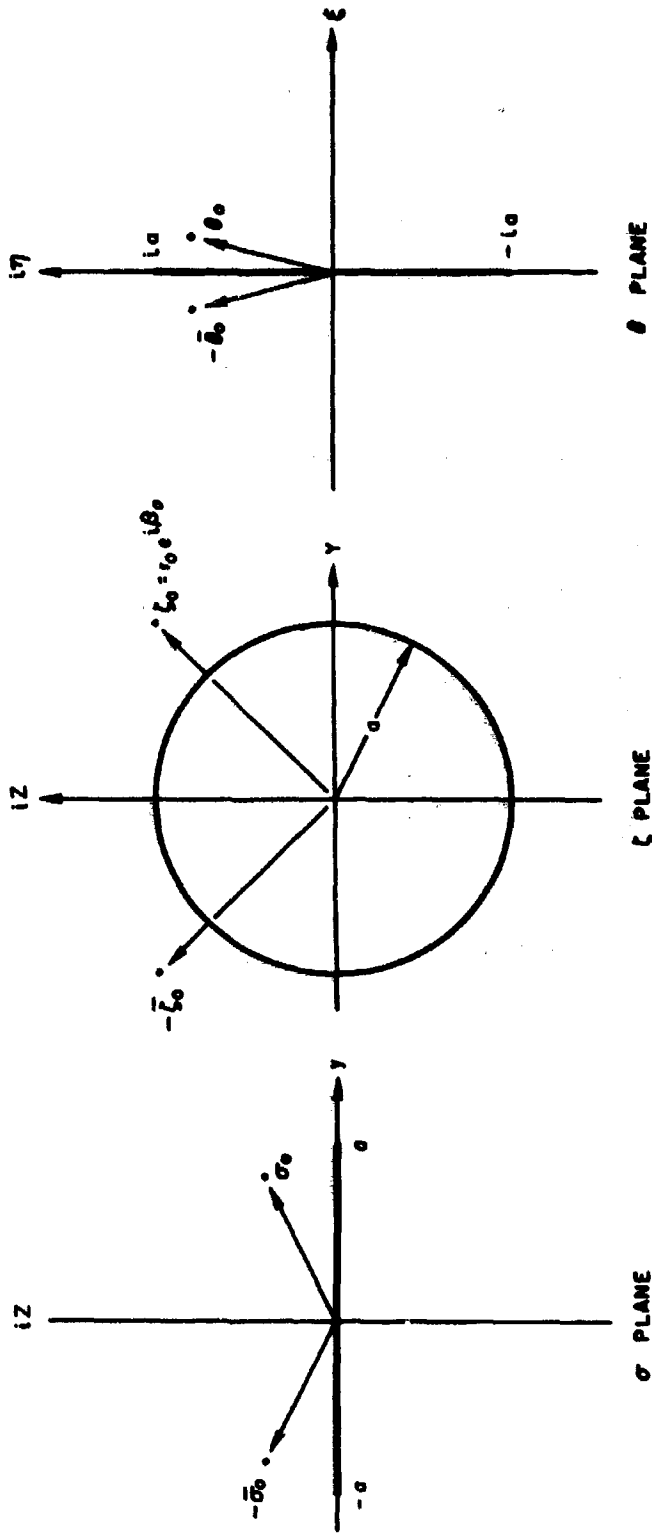


Figure 4. Generation of the Concentrated Vortex.



The wing in the  $\sigma$  plane can be mapped into a circle of radius  $a$  with its center at the origin in the  $\zeta$  plane by use of the transformation

$$\zeta = \sigma \pm \sqrt{\sigma^2 - a^2} \quad (9)$$

with the sign changing from upper to lower surface. The vector distance in the  $\zeta$  plane is given by

$$\zeta = Y + iZ \quad (10)$$

or in polar form

$$\zeta = re^{i\beta} \quad (11)$$

The wing can also be mapped onto the imaginary axis of the  $\theta$  plane by use of the transformation

$$\theta = \sqrt{\sigma^2 - a^2} \quad (12)$$

where

$$\theta = \xi + i\eta \quad (13)$$

The complex potential for the desired vortex flow in the  $\theta$  plane is given by

$$W(\theta) = -\frac{ik}{2\pi} [\ln(\theta - \theta_0) - \ln(\theta + \bar{\theta}_0)] - iUa\theta \quad (14)$$

By application of Eq. (12), the complex potential in the physical plane is obtained.

$$W(\sigma) = \frac{-ik}{2\pi} \left\{ \ln \left[ \sqrt{\sigma^2 - a^2} - \sqrt{\sigma_0^2 - a^2} \right] - \ln \left[ \sqrt{\sigma^2 - a^2} + \sqrt{\sigma_0^2 - a^2} \right] \right\} - iUa\sqrt{\sigma^2 - a^2} \quad (15)$$

In the circle plane, the complex potential becomes

$$W(\zeta) = \frac{-ik}{2\pi} \left[ \ln(\zeta - \zeta_0) \left( \zeta + \frac{a^2}{\zeta_0} \right) - \ln(\zeta + \zeta_0) \left( \zeta - \frac{a^2}{\zeta_0} \right) \right] - \frac{iUa}{2} \left( \zeta - \frac{a^2}{\zeta} \right) \quad (16)$$

Equations (14), (15), and (16) represent the wing in its appropriately transformed state immersed in a uniform flow of velocity  $U\alpha$  in the  $\sigma$  and  $\theta$  plane and  $Ua/2$  in the  $\zeta$  plane with two vortices of strength  $\pm k$  disposed symmetrically about the imaginary axis.

The vortex position and strength are now obtained by forming the expression

$$(v_0 - iw_0)^* = \lim_{\sigma \rightarrow \sigma_0} \frac{\partial}{\partial \sigma} \left[ W(\sigma) + \frac{ik}{2\pi} \ln(\sigma - \sigma_0) \right] \quad (17)$$

Performing this operation and adding  $-U\epsilon(\bar{\sigma}_0/a)$ , Eq. (6) becomes

$$\frac{ik}{2\pi} \left\{ \frac{\sigma_0}{\left( \sigma_0^2 - a^2 \right) + \sqrt{\sigma_0^2 - a^2} \sqrt{\bar{\sigma}_0^2 - a^2}} + \frac{a^2}{2\sigma_0 \left( \sigma_0^2 - a^2 \right)} \right\} - \frac{iUa\sigma_0}{\sqrt{\sigma_0^2 - a^2}} - \frac{U\epsilon\bar{\sigma}_0}{a} = 0 \quad (18)$$

By separating Eq. (18) into its real and imaginary parts and introducing the remaining boundary condition,

$$\frac{z_0}{a} = \frac{1}{4} \frac{a}{\epsilon} \quad (19)$$

two equations are obtained which, when solved simultaneously, yield the solution for the normalized vortex spanwise location  $y_0/a$  and strength  $k/2\pi Ua\epsilon$  as a function of  $a/\epsilon$ .

The resultant set of equations is not amenable to analytic solution and, therefore, a numerical technique was used. Two nontrivial solutions for  $y_0/a$  were found to exist (see Fig. 6). The primary solution starts at the wing leading edge and moves rapidly inboard to a minimum spanwise position of  $y_0/a = 0.55$ . The vortex then travels upward and outboard to a maximum height of  $z_0/a = 0.605$ . The secondary solution starts at the wing leading edge but deviates only slightly in its lateral position with increasing  $a/\epsilon$  to form a gentle backward S curve and form a closed loop with the primary branch. The primary branch conforms to experiment in the low and middle range of  $a/\epsilon$ . The upper part of the primary branch, where the vortex swings sharply outboard, has no verification in experiment and is considered the region in which the model tends to weaken. The secondary branch does not conform to experience over most of its range and is rejected in its entirety.

The solutions of Brown and Michael, Legendre, and Mangler and Smith, as well as a limited number of test points, are also shown in Fig. 6. These curves are to the right of the experimental data and all fail to predict the very rapid inboard travel of the vortex at small  $a/\epsilon$ .

Because of the limited data on vortex lateral and vertical position, a second correlation has been attempted as shown in Fig. 7. Only the vortex lateral position is presented, as determined by flow visualization studies and surface pressure distributions. The test data form a band the lefthand side of

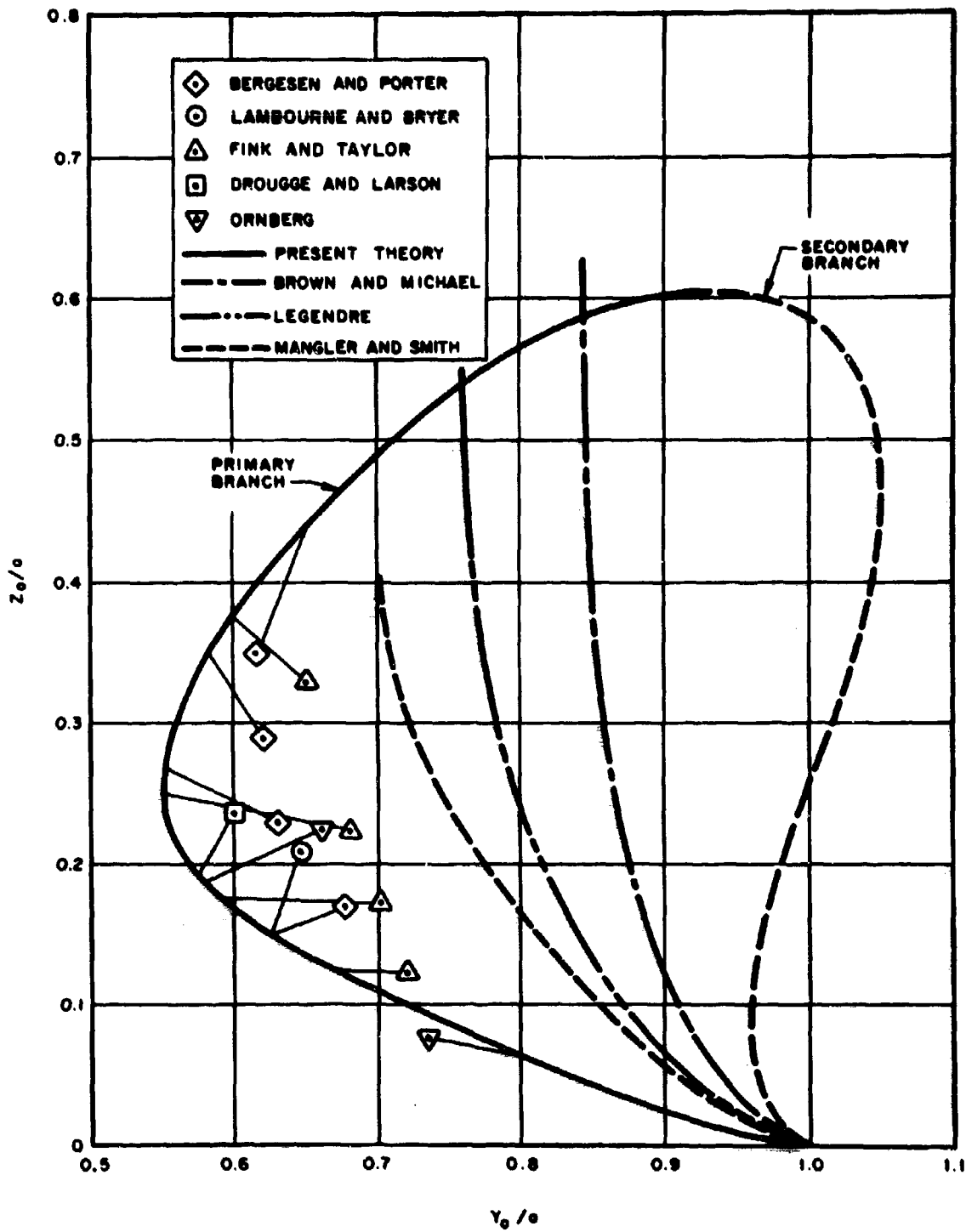


Figure 6. Computed Vortex Location.

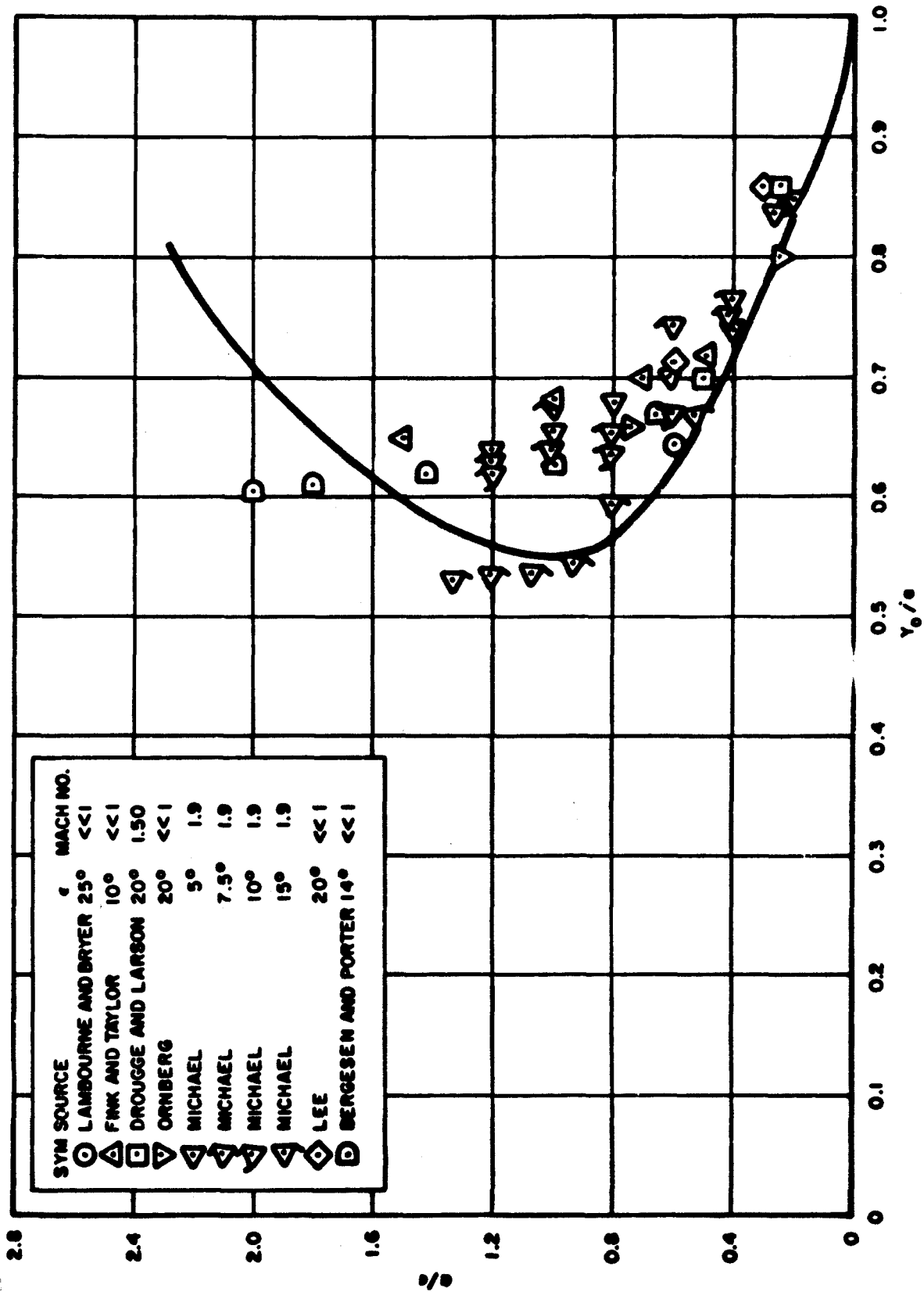


Figure 7. Comparison of Calculated and Measured Vortex Lateral Position.

which is bounded by the present solution for vortex location. In the lower ranges of  $a/\epsilon$ , the predicted rapid inboard movement of the vortex is satisfactorily verified by the data. The width of the band here and in subsequent correlations is attributed to normal scatter in reducing the data, the variation in leading edge condition, and the wide range of aspect ratio and Mach number.

Figure 8 presents the variation of vortex strength with  $a/\epsilon$  for the primary and secondary branches. The secondary branch solution yields higher values of  $k/2\pi Ua\epsilon$  for all  $a/\epsilon$  and would therefore indicate higher values of kinetic energy in the surrounding fluid. On this basis, the rejection of the secondary branch seems consistent since the configuration representing the lowest energy state is expected to be found in nature.

#### D. CALCULATION OF THE FORCE ON THE WING

The force acting on the wing is first obtained from momentum considerations; the wing surface plus the lines joining the leading edge to the concentrated vortices are used as the contour of integration, as in Ref. 4. Converting to coefficient form  $C_L/\epsilon^2$  we obtain, in circle plane notation,

$$\frac{L}{\rho U^2 a \epsilon} = \frac{C_L}{\epsilon^2} = 2\pi \left[ \frac{a}{\epsilon} + \frac{2}{r_o a} \left( \frac{k}{2\pi U a \epsilon} \right) (r_o^2 - a^2) \cos \beta_o \right] \quad (20)$$

The first term of Eq. (20),  $2\pi a/\epsilon$ , corresponds to the slender wing theory of Jones. Within the small angle approximation,  $\epsilon = AR/4$  and the first term reduces to the familiar  $\pi AR/2$ . The remaining terms involving  $k$  are the nonlinear contribution to the lift coefficient. Equation (20) is plotted in Fig. 9 along with the solutions of Jones, Brown and Michael, and Legendre. The solution is seen to be always greater than the linear theory but less than that of Brown and Michael.

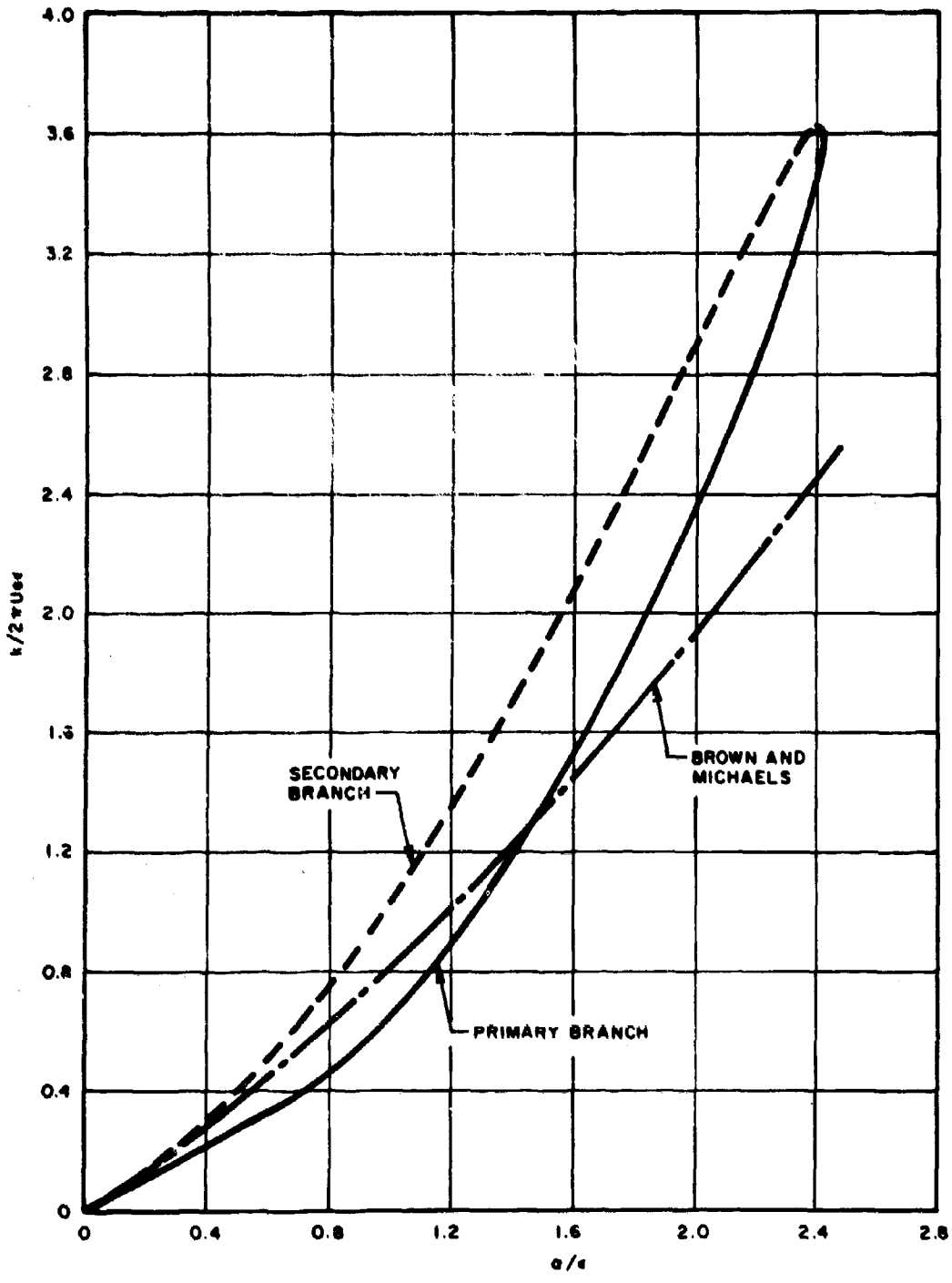


Figure 8. Variation of Vortex Strength With Angle-of-Attack.

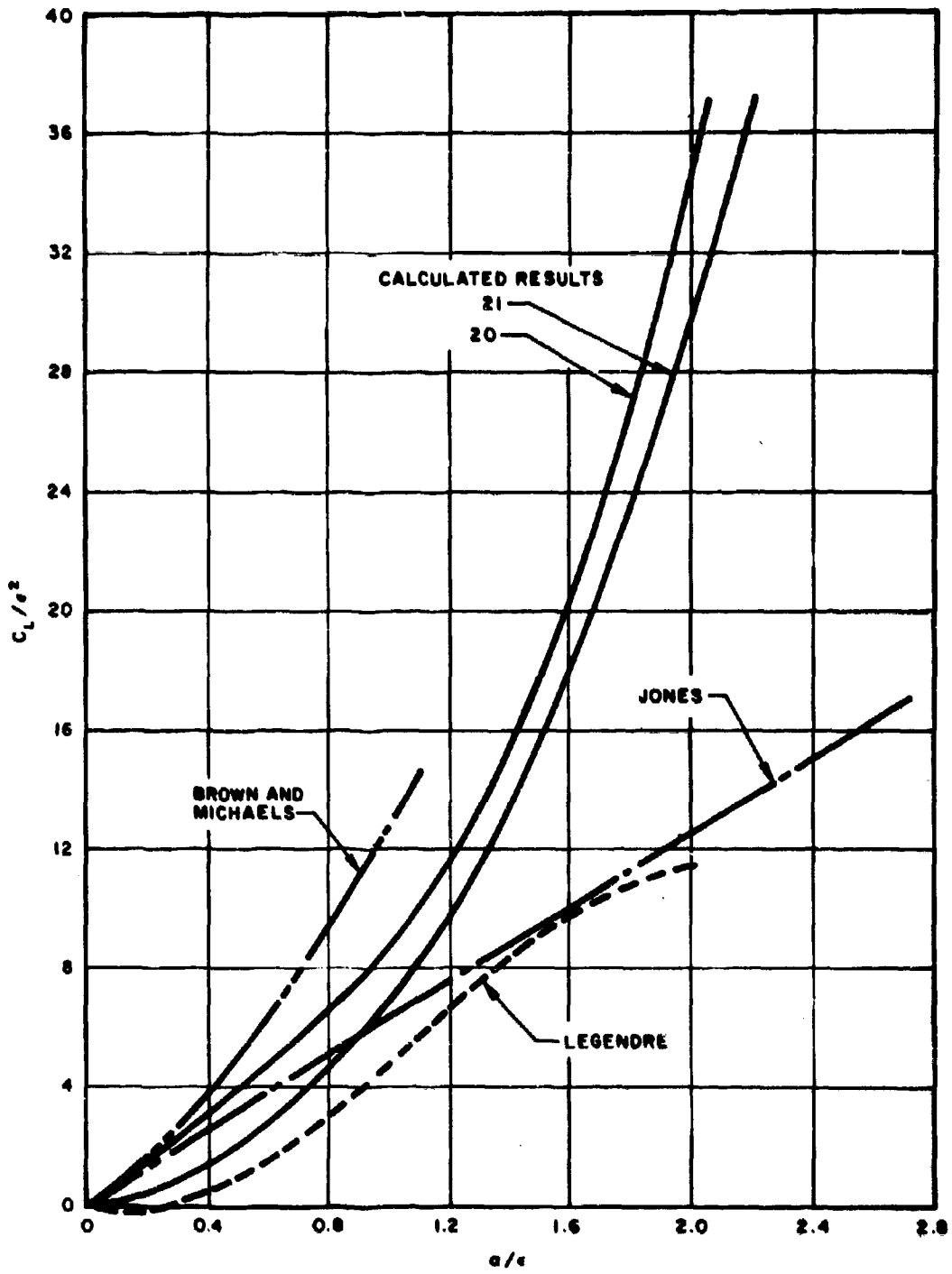


Figure 9. Calculated Lift Coefficient.

The lift can also be computed by use of the unsteady form of Blasius' theorem using the wing surface as the contour of integration. For the lift coefficient this procedure yields

$$\begin{aligned}
 \frac{C_L}{2} = 2\pi \left\{ \left[ \frac{a}{\epsilon} - \frac{4a}{r_o} \left( \frac{k}{2\pi U a \epsilon} \right) \cos \beta_o \right] \right. \\
 + 2a r_o \left( \frac{k}{2\pi U a \epsilon} \right) \sin \beta_o \left[ \frac{(r_o^2 - a^2) [(r_o^2 + a^2)^2 + 4a^2 r_o^2 \cos^2 \beta_o]}{[(r_o^2 - a^2)^2 + 4a^2 r_o^2 \sin^2 \beta_o]^2} \right. \\
 + \frac{2a^2 [a^4 + 4r_o^4 \cos^2 \beta_o]}{(r_o^4 - a^4)^2 + 16a^4 r_o^4 \sin^2 \beta_o \cos^2 \beta_o} \\
 \left. \left. + \frac{a^4 - r_o^4 + 4a^2 r_o^2}{(r_o^2 - a^2) [(r_o^2 - a^2)^2 + 4a^2 r_o^2 \sin^2 \beta_o]} \right] \right. \\
 \left. - 8 \frac{a}{\epsilon} \left( \frac{k}{2\pi U a \epsilon} \right) \frac{a^2 r_o^2 \sin \beta_o \cos \beta_o}{[(r_o^2 - a^2)^2 + 4a^2 r_o^2 \sin^2 \beta_o]} \right\} \quad (21)
 \end{aligned}$$

which also consists of the linear term  $2\pi a/\epsilon$  and the nonlinear terms contributed by the vortex. Equation (21) is also plotted in Fig. 9 and is seen to fall below the linear theory of Jones in the low range of  $a/\epsilon$ . This characteristic is a consequence of the vortex model employed and is displayed in the results of Legendre to an even greater degree.

A comparison of the various theories, with test data covering a wide range of aspect ratios, yields unsatisfactory correlation. The data form a wide band with the solution of Brown and Michael as an upper limit and many points lying on or below the linear theory. The scatter is so great that no conclusions seem possible. The reason for the scatter can be found by noting that the Jones linear theory deteriorates in accuracy for aspect ratios much greater than unity. For example, at aspect ratio 1, the Jones value of  $C_{L\alpha}$  is over 20 percent greater than that predicted by the more accurate theory of Ref. 12. This deviation is of the same order of magnitude as the nonlinear term of Eq. (20) and tends to mask it. Since the nonlinear characteristics of the theory are of interest here, it is considered that a correlation with the linear contribution removed is of greatest significance. Such a correlation is shown in Fig. 10 where the nonlinear terms of Eq. (20) and of Brown and Michael as well as the nonlinear components of test data are presented.

The  $\alpha/\epsilon$  axis of Fig. 10 represents the Jones theory. The data now form a band for which the mean value is well represented by Eq. (20) up to  $\alpha/\epsilon \cong 1.2$ . Within the low and medium range of  $\alpha/\epsilon$ , the correlation is good considering the nature of the simplifications made in the model and the simulation rather than actual representation of the secondary vortex system. These results indicate the importance of the secondary vortex system in the accurate prediction of the nonlinear forces.

#### E. PRESSURE DISTRIBUTION AND SPAN LOADING

The unsteady form of Bernoulli's equation which is applicable to the cross-flow plane is

$$\frac{P_{\infty}}{\rho} + \frac{1}{2} U^2 \alpha^2 = C(t) = \frac{p}{\rho} + \frac{1}{2} q^2 + \frac{\partial \Phi}{\partial t} \quad (22)$$

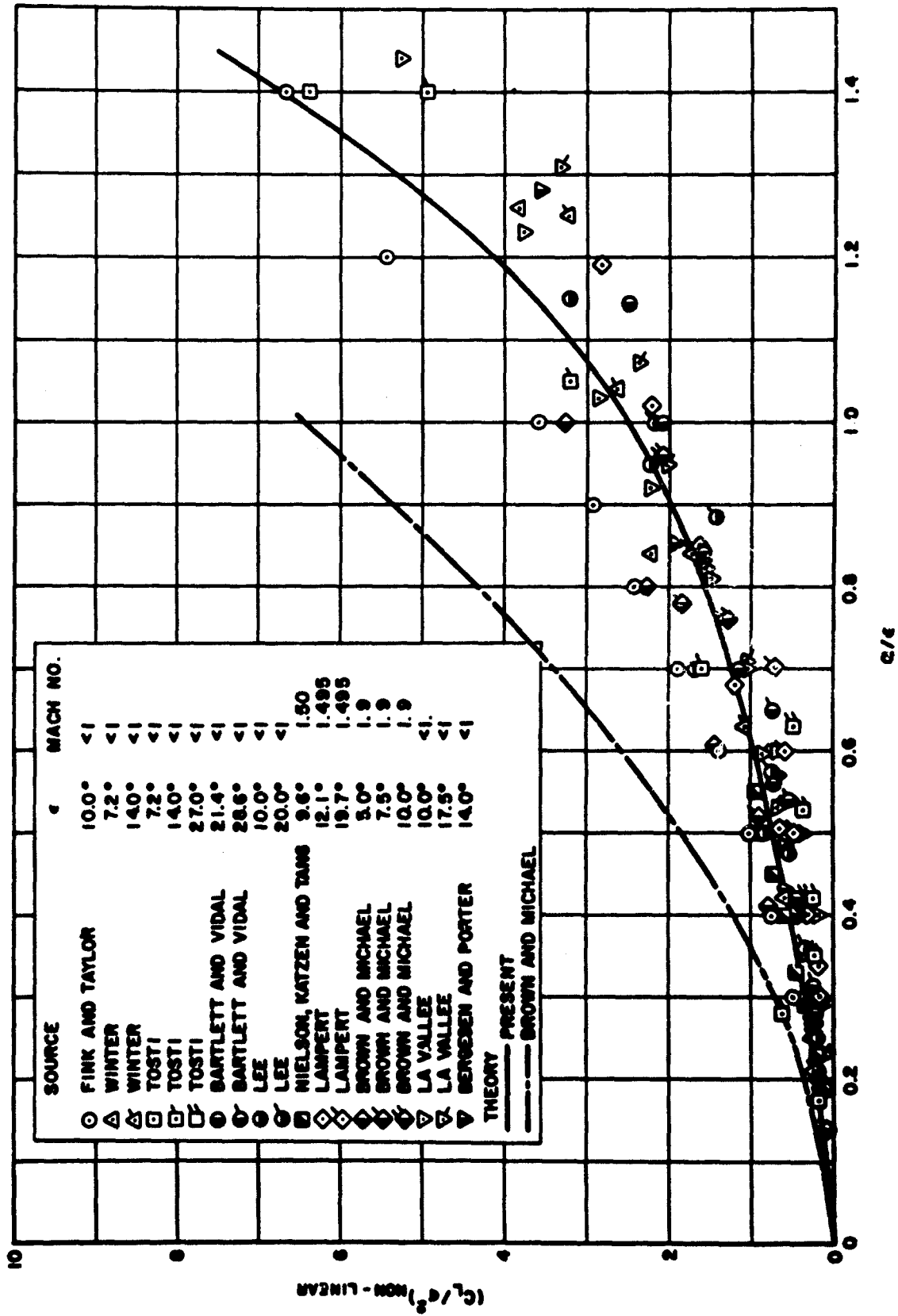


Figure 10. Comparison of Computed and Measured Nonlinear Component of Lift Coefficient.

By rearrangement of terms, the pressure coefficient is obtained in the form

$$\frac{C_p}{2} = \left(\frac{a}{\epsilon}\right)^2 - \left(\frac{q}{U\epsilon}\right)^2 - \frac{1}{U\epsilon} \frac{\partial(W + \bar{W})}{\partial a} \quad (23)$$

The second term of Eq. (23) is the ratio of the cross-flow velocity  $q$  to the component of free stream velocity perpendicular to the wing leading edge. The term is obtained by differentiating Eq. (15) with respect to  $\sigma$ , evaluating at the wing surface, and dividing by  $U\epsilon$ . The last term of Eq. (23), the time dependent part of the pressure coefficient, is obtained from Eq. (16). Combining all terms, the pressure coefficient is given by

$$\begin{aligned} \frac{C_P}{\epsilon^2} = & \left(\frac{a}{\epsilon}\right)^2 - \left\{ \frac{\cos \beta}{\sin \beta} \left[ \left(\frac{k}{2\pi U a \epsilon}\right) \frac{\cos \beta_o (r_o^2 - a^2)}{\frac{r_o}{a} f(\beta)} - \frac{a}{\epsilon} \right] \right\}^2 \\ & - 2 \left(\frac{k}{2\pi U a \epsilon}\right) \left\{ \frac{-4 \cos \beta}{\sin \beta} [\Sigma_1 + \Sigma_2] + 4 [\Sigma_3 - \Sigma_4] \pm \pi + 2\beta_o \right\} - \frac{2}{\sin \beta} \frac{a}{\epsilon} \end{aligned} \quad (24)$$

where

$$\begin{aligned} f(\beta) = & a^2 \sin^2 \beta - \frac{a}{r_o} (r_o^2 + a^2) \sin \beta \sin \beta_o \\ & + \frac{1}{4r_o^2} [(r_o^2 - a^2)^2 + 4r_o^2 a^2 \sin^2 \beta_o] \end{aligned} \quad (25)$$

$$\begin{aligned}
\Sigma_1 &= \sum_{n=1}^{\infty} \left(\frac{a}{r_0}\right)^{(2n-1)} \cos(2n-1)\beta \cos(2n-1)\beta_0 \\
\Sigma_2 &= \sum_{n=1}^{\infty} \left(\frac{a}{r_0}\right)^{2n} \sin 2n\beta \sin 2n\beta_0 \\
\Sigma_3 &= \sum_{n=1}^{\infty} \frac{1}{2n} \left(\frac{a}{r_0}\right)^{2n} \cos 2n\beta \sin 2n\beta_0 \\
\Sigma_4 &= \sum_{n=1}^{\infty} \frac{1}{(2n-1)} \left(\frac{a}{r_0}\right)^{(2n-1)} \sin(2n-1)\beta \cos(2n-1)\beta_0
\end{aligned} \tag{26}$$

and the sign of  $\pi$  changes in going from the upper to the lower surface.

For small values of  $a/\epsilon$ ,  $\Sigma_1$  and  $\Sigma_2$  converge very slowly and can be replaced by

$$\Sigma_1 + \Sigma_2 = \frac{(r_0^2 - a^2)}{4} \left[ \frac{1}{r_0^2 + a^2 - 2ar_0 \cos(\beta - \beta_0)} - \frac{1}{r_0^2 + a^2 + 2ar_0 \cos(\beta + \beta_0)} \right] \tag{27}$$

By setting  $(k/2\pi Ua\epsilon)$  equal to zero, the slender wing solution of Ref. 9 is recovered.

The pressure coefficient can be expressed as a function of the wing semi-span  $y/a$  by use of the relationship  $y/a = \cos \beta$ , and is shown in Fig. 11 with the solution of Brown and Michael and the test results of Fink and Taylor (Ref. 13).

The pressure coefficient of the present theory displays somewhat different characteristics from those of Brown and Michael (Fig. 11a),

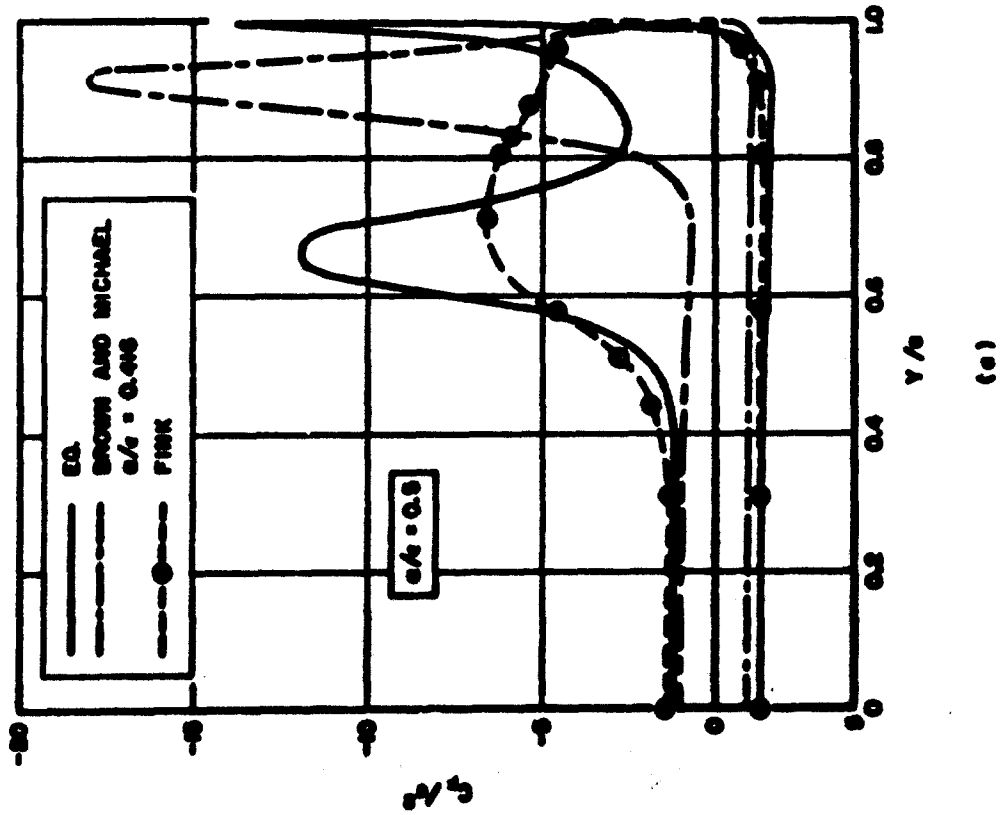
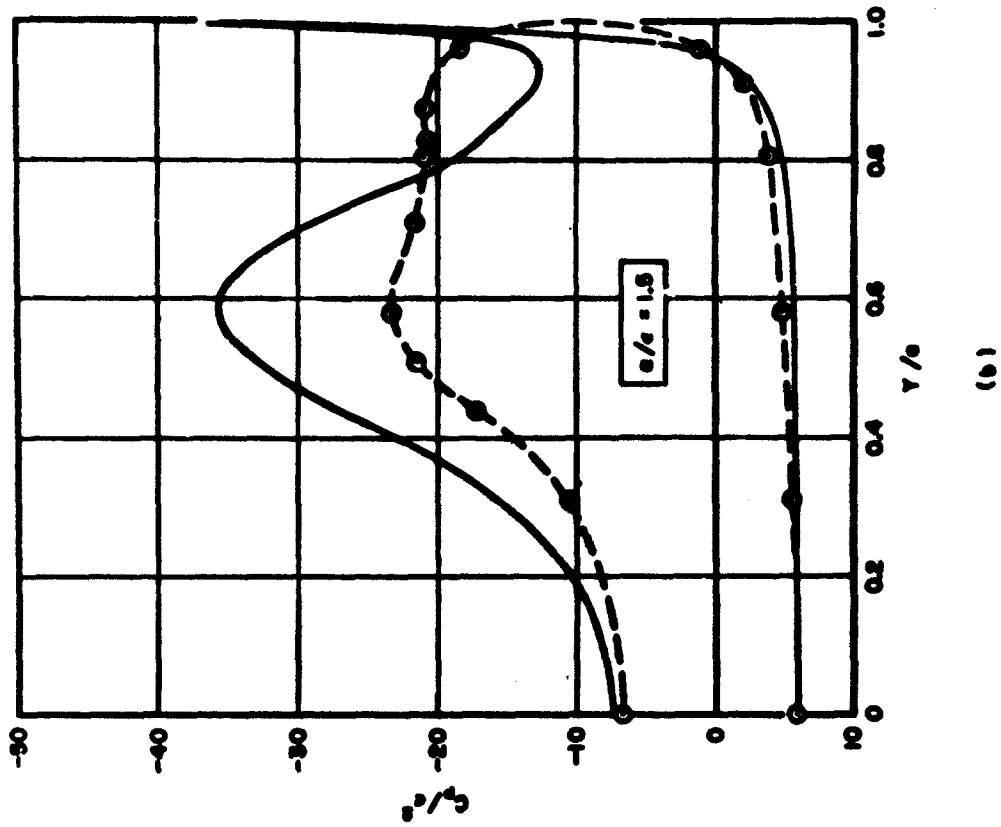


Figure 11. Comparison of Calculated and Measured Pressure Coefficient.

primarily in the position of the negative pressure peak and behavior at the leading edge. Test data verify the inboard position of the pressure peak and the pressure plateau at the leading edge but the magnitude of the pressure peaks is overestimated by both theories. It is of interest to note that even at high values of  $a/\epsilon$ , where the predicted force coefficient tends to diverge from experiment, very good correlation of pressure coefficient is obtained (Fig. 11b).

The calculated value of normalized span loading for  $a/\epsilon = 0.8$  is presented in Fig. 12. The theories of Jones, and Brown and Michael, and the data of Ref. 14 are also shown for comparison. The characteristics of primary interest are the large deviation between the calculated curve of the present analysis and the elliptic loading and the good correlation with experiment.

#### F. STREAMLINES AND STAGNATION POINTS

The streamlines in the cross-flow plane can be obtained from the complex potential  $W = \Phi + i\psi$  [Eq. (14)] by obtaining the expression for  $\psi$  and setting it equal to a constant. In the  $\theta$  plane, the normalized stream function  $\psi/Ua\epsilon$  is

$$\frac{\psi}{Ua\epsilon} = -\left(\frac{k}{2\pi Ua\epsilon}\right) \ln \frac{\rho_1}{\rho_2} - \frac{a}{\epsilon} \frac{\xi}{a} \quad (28)$$

where

$$\rho_1 e^{i\lambda_1} = \theta - \theta_0 \quad ; \quad \rho_2 e^{i\lambda_2} = \theta + \bar{\theta}_0 \quad (29)$$

Rearranging terms

$$\frac{\rho_2}{\rho_1} = \exp \left\{ \left[ \frac{\psi}{Ua\epsilon} + \frac{a}{\epsilon} \frac{\xi}{a} \right] / \left( \frac{k}{2\pi Ua\epsilon} \right) \right\} \quad (30)$$

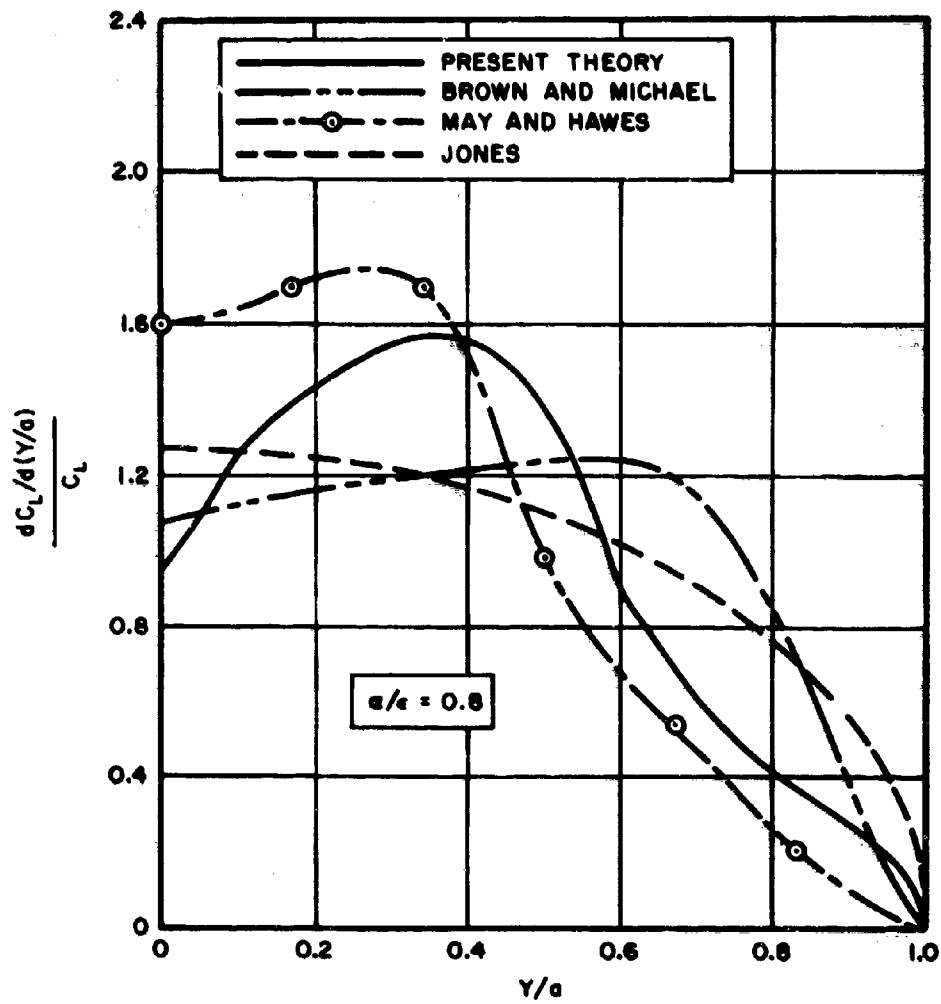


Figure 12. Comparison of Computed and Measured Span Loadings.

The interpretation of Eq. (30) is shown in Fig. 13; from its geometry, the relationship between the  $\theta$  plane coordinates can be obtained in the form

$$\eta = \eta_0 \pm \left[ \frac{4\xi\xi_0}{\exp 2 \left[ \frac{\psi}{Ua\epsilon} + \frac{a}{\epsilon} \frac{\xi}{a} \right] / \left( \frac{k}{2\pi Ua\epsilon} \right) - 1} - (\xi - \xi_0)^2 \right]^{1/2} \quad (31)$$

The computed streamline patterns for  $a/\epsilon = 0.25$  are shown in Fig. 14 in both the  $\theta$  and  $\sigma$  plane.

The stagnation lines are defined as those generating lines of the delta wing which are not crossed by surface streamlines. They are obtained by equating the slope of the surface streamline to the slope of the generating line  $\epsilon \cos \beta$  and solving for  $\beta$ . The surface streamline slope  $q/U$  is obtained directly from Eq. (24). The computed stagnation lines are shown in Fig. 15 with a limited amount of test data. The inboard stagnation point travels rapidly toward the wing centerline and rises along the  $z$  axis with increasing  $a/\epsilon$  while the outboard stagnation point travels slowly inboard to a minimum value of  $y/a = 0.80$  and moves outboard again with increasing  $a/\epsilon$ . It is interesting to note that the theoretically predicted reversal of spanwise travel of the outboard stagnation line is verified in the test data of Lee (Ref. 15), and for the high Reynolds number data, the quantitative correlation at low and intermediate  $a/\epsilon$  is quite good. Extrapolation of the test data for  $y/a = 1$  yields values of  $a/\epsilon$  on the order of 0.2 - 0.3 rather than zero. This is because, even for sharp leading edge planforms, test results show no leading edge separation at the initial angles of attack. The data of Ref. 13, for example, show attached flow up to a value of  $a/\epsilon = 0.3$ . The data for the inboard stagnation point substantiate the theoretical curve satisfactorily for the low and intermediate values of  $a/\epsilon$ . At the higher values, the deviation of Lee's data is attributed to the effects of the center-body mounted on the test model.



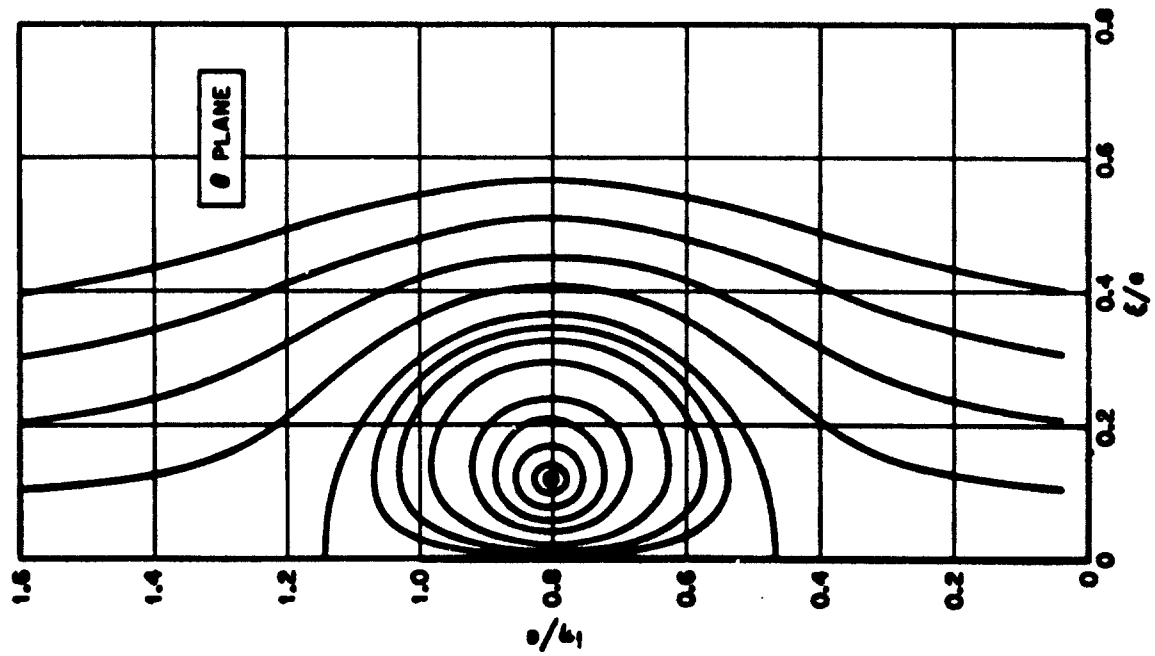
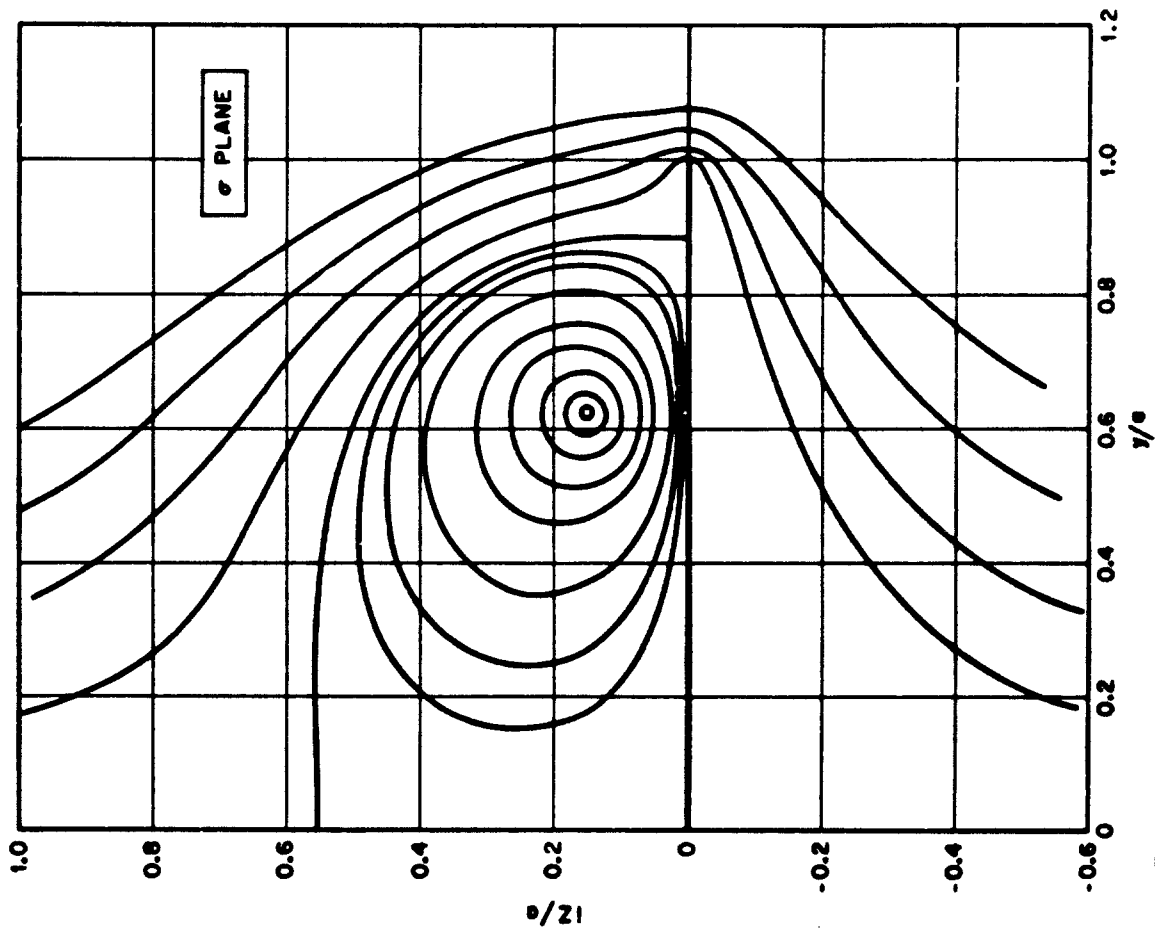


Figure 14. Streamline patterns in the  $x/e$  vs  $z/e$  and  $y/e$  vs  $z/e$  planes.

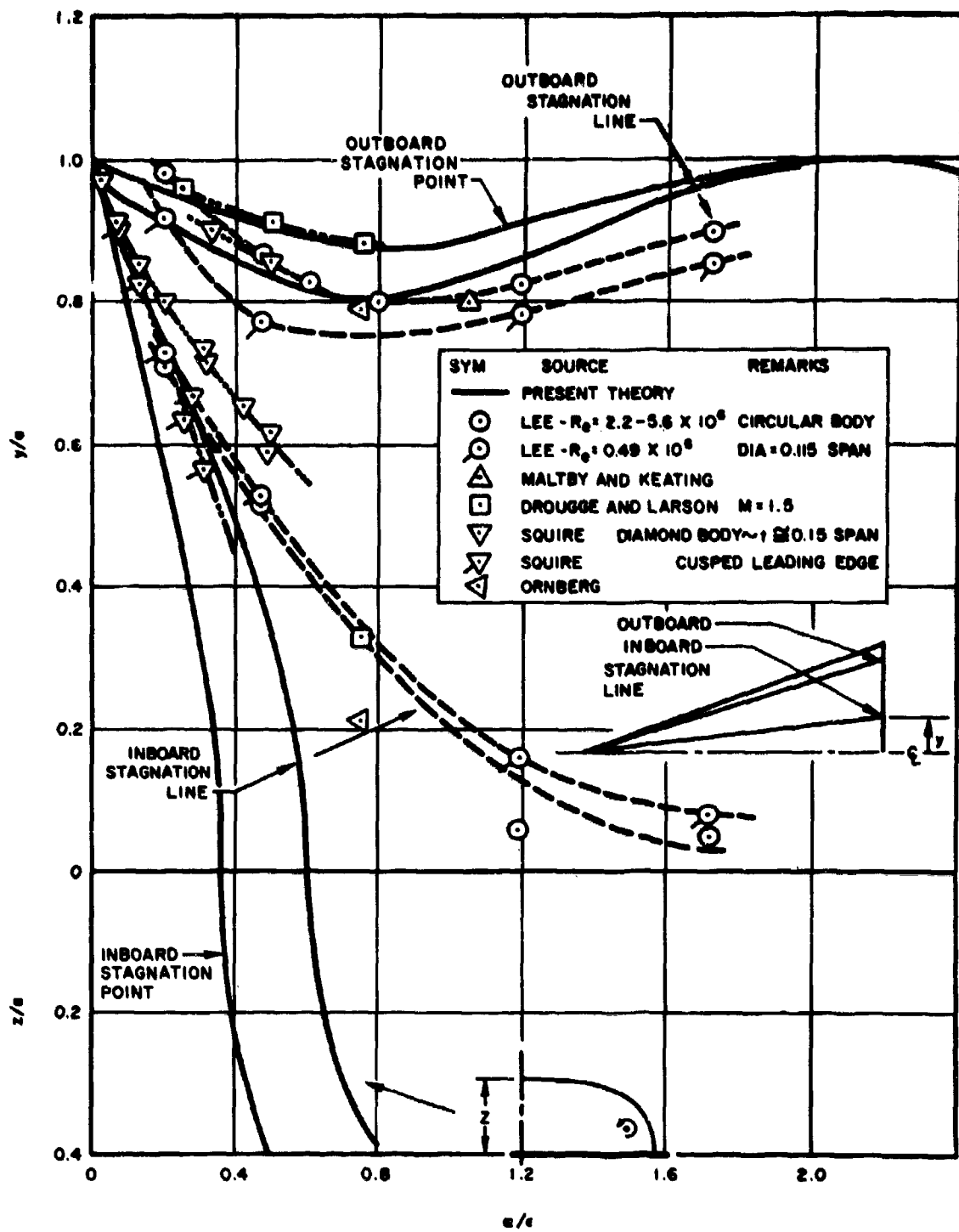


Figure 15. Stagnation Line Location.

In the two-dimensional cross-flow plane, the points at which the  $(\psi/Ua\alpha) = 0$  streamline impinge on the wing surface are stagnation points and may be obtained from Eq. (31) by taking the limit as  $\xi$  approaches zero. The stagnation points are then given by

$$\eta_{\text{stagnation}} = \eta_o \pm \left[ \frac{2a\xi_o \left( \frac{k}{2\pi Ua\epsilon} \right) - \xi_o^2}{a/\epsilon} \right]^{1/2} \quad (32)$$

Equation (32), transformed to the  $\sigma$  plane, is also shown in Fig. 15.

The effectiveness of the outboard stagnation point in qualitatively introducing the effects of the secondary vortex system can be clearly seen by an inspection of the complete surface streamline pattern in the plane of the wing. The surface streamlines are obtained directly from Eq. (24) and two cases are shown in Fig. 16. These flow patterns show the characteristics of multiple stagnation lines, herringbone patches and, at the lower angles of attack, nearly uniform chordwise flow over the center section. These characteristics are typical of those found in flow visualization tests (Refs. 1 and 2).

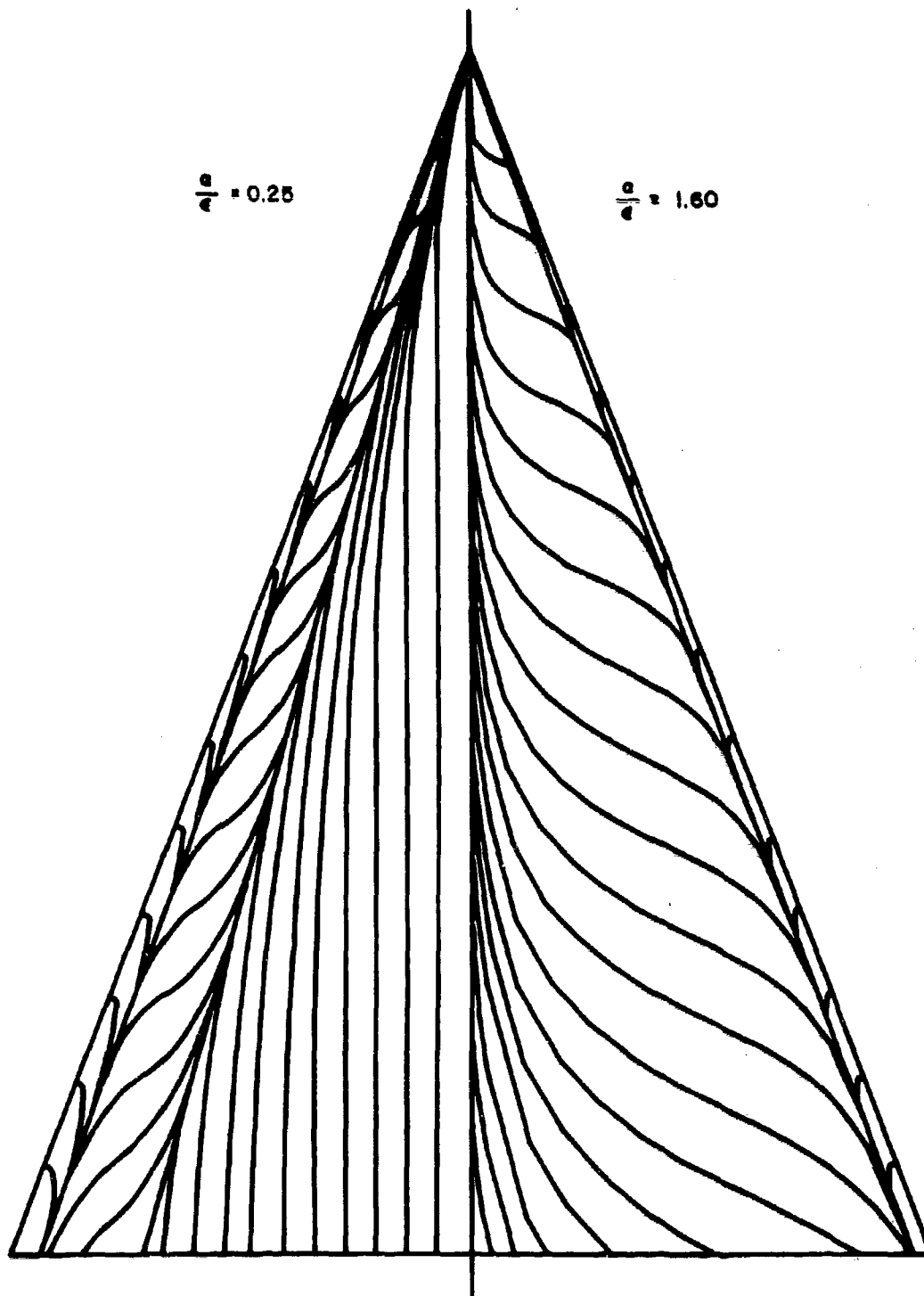


Figure 16. Computed Surface Streamlines on a  $20^\circ$  Delta Wing.

### III. DISCUSSION OF RESULTS

A comparison of the present model of flow about sharp edge deltas with separation has been made with previous models and with experiment. A review of the results obtained indicates that the existence of the outboard stagnation point results in a simulation of the effects of secondary vortex formation near the wing leading edge. As a result, a more satisfactory correlation of nonlinear lift, vortex position, pressure distribution, and span loading and flow pattern is obtained with experiment over the range of  $\alpha/\epsilon$  than was obtained with previous analyses. However, the analytic solution for lift is multi-valued and it tends to diverge from experiment in the high  $\alpha/\epsilon$  range.

All of the models considered herein possess inherent deviations from the physical flow. These deviations are a consequence of the mathematical simplifications made in attacking the problem through slender wing techniques and in reducing the viscous phenomena to models readily amenable to analytic treatment. The use of slender wing theory restricts the range of aspect ratio and Mach number. Furthermore, the assumption of conical flow is not completely accurate in the subsonic region. The experiments of Fink and Taylor (Ref. 13) show that at low speeds a large region of conical flow exists near the wing apex but the flow tends to become nonconical near the trailing edge. Some error is introduced into the analysis when the vorticity field is represented by a concentrated filament. It is argued that the vortex core so dominates the flow that the vorticity field seems a concentrated filament to the wing surface. In spite of the small amount of vorticity contained in the vortex sheet, its effect is not completely negligible because of its proximity to the wing leading edge. This is shown by a comparison of the Brown and Michael model with that of Mangler and Smith. The two models differ primarily in their description of the vortex sheet, and the effect on predicted lift and vortex position is significant.

It is considered that the most important source of error inherent in previous analyses is the omission of secondary vortex formation effects. The importance of the secondary vortex system on sharp edge surfaces is a function of the component of free stream velocity perpendicular to the wing leading edge  $U\epsilon$  (see Ref. 8). In a plane perpendicular to the leading edge, the vector sum of  $U\epsilon$  and  $U\alpha$  form an angle  $\omega$  with the surface of the wing. The angle  $\omega$  has a large effect on the position of the concentrated vortex and its strength. A qualitative measure of vortex strength can be obtained from Fig. 17 which presents the drag coefficient of a two-dimensional wedge as a function of  $\omega$ . To first order, the drag coefficient is a measure of the vortex strength and is shown to increase with increasing  $\omega$ . The effect of planform shape on  $\omega$  is represented schematically in Fig. 18. For the delta planforms considered,  $\epsilon$  is positive and  $U\epsilon$  represents a velocity vector directed inboard from the leading edge (Fig. 18a). The angle  $\omega$  (being greater than  $\pi/2$ ) forces the concentrated vortices inboard where they generate high adverse spanwise pressure gradients and separated boundary layer flow. The vorticity, with its outboard movement restricted by  $U\epsilon$ , tends to build up and modify the entire flow field about the wing. A delta planform with apex pointed downstream has negative  $\epsilon$  (Fig. 18b) and  $U\epsilon$  directed outboard. The swept sides now act as trailing edges and  $\omega$  is less than  $\pi/2$ . The concentrated vortices are forced outboard and their strength is less than the previous case. Spanwise pressure gradients are correspondingly weaker and the boundary layer generated vorticity tends to be washed off the wing, thereby reducing its influence on the flow field. As  $\alpha/\epsilon$  approaches zero, the flow corresponds to that of a high aspect ratio tapered wing. In this case, the success of potential theory attests to the minor influence of secondary flow phenomena.

The present theory must be considered a simplified model which represents the effects of secondary vortex separation only qualitatively. Instead of introducing the secondary vortices explicitly into the mathematical model, the boundary conditions have been adjusted to simulate their presence.

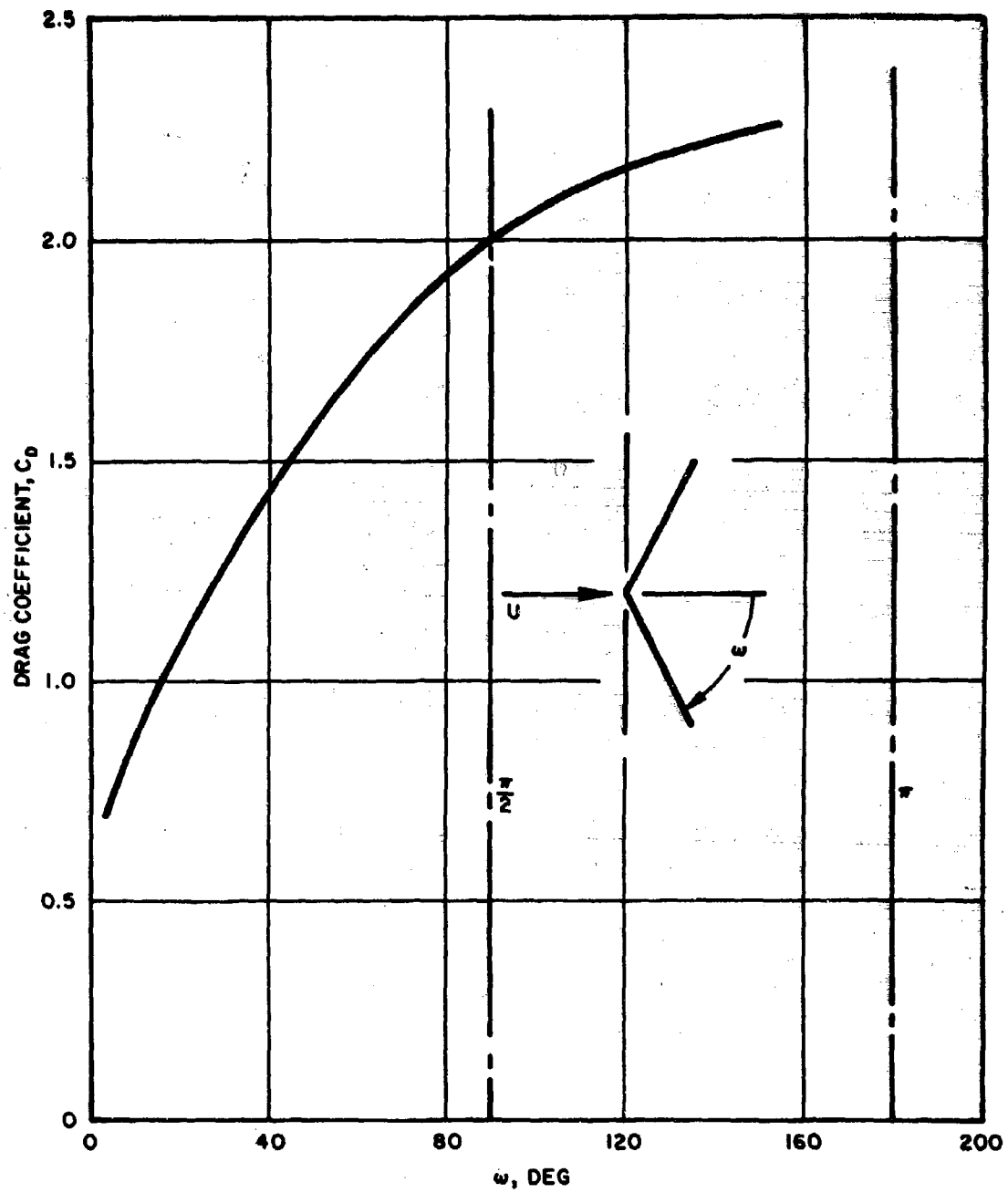
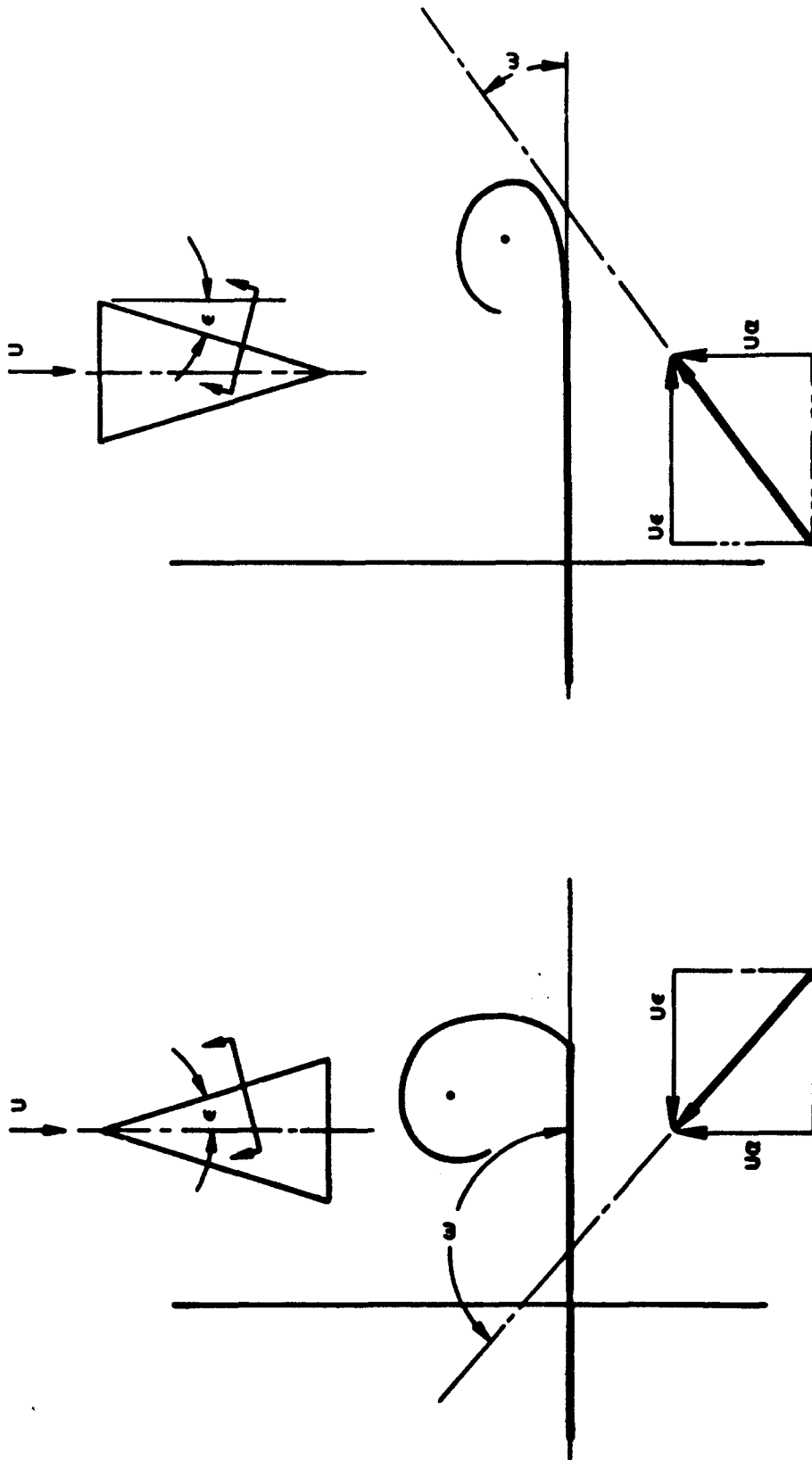


Figure 17. Drag Coefficient of a Two Dimensional Wedge.



(b)  $\epsilon$  LESS THAN ZERO

(a)  $\epsilon$  GREATER THAN ZERO

Figure 18. Flow in the Plane Perpendicular to the Leading Edge.

This procedure simplifies the analysis, and will not yield results which are as accurate or valid over as large a range of  $a/\epsilon$  as a more sophisticated approach. It does, however, display the basic characteristics of this type of flow and demonstrates the necessity for including the effects of secondary separation.

#### IV. CONCLUSIONS

An approximate theory for the flow about slender delta wings with sharp leading edges, qualitatively incorporating the effects of secondary separation, leads to the following conclusions:

1. Over the range of  $\alpha/\epsilon$ , the secondary vortex simulation yields improvements over previous theories in the prediction of the flow field characteristics as indicated by the correlation of calculated vortex position and streamline pattern with test data. The concentrated vortices are shown to move rapidly inboard with initial increase in  $\alpha/\epsilon$  in accordance with experimental observations. At the high values of  $\alpha/\epsilon$  there is divergence of vortex position from test data.
2. The solution for the nonlinear component of the lift coefficient correlates well with the nonlinear component of test data.
3. The calculated pressure distributions correlate well with test data over the range of  $\alpha/\epsilon$ . The lateral position and magnitude of the negative pressure peak and the outboard negative pressure plateau are predicted more accurately than with previous theories.

## APPENDIX

### THE FORCE-FREE VORTEX SYSTEM

The concentrated vortex feeding sheet system can be rendered force-free by locating the concentrated vortex and its planar feeding sheet such that the forces on each are of an equal but opposite magnitude. This leads to an expression similar to Eq. (6) with the term  $(\sigma_0/a)U\epsilon$  replaced by  $(2\sigma_0 - a)U\epsilon/a$ . The term  $(2\sigma_0 - a)U\epsilon/a$  now represents the velocity of the center of gravity of a vortex system, this can be seen from Fig. 4a. None of the vortex filaments of Fig. 4a are generated with conical symmetry except that filament originating at the wing apex. Using the previous notation for vorticity center of gravity position in the cross-flow plane, the vector velocity of the apex-generated filament is  $(2\sigma_0 - a)U\epsilon/a$ . All other filaments generated along the leading edge lie parallel to the apex filament and have a velocity equal to it. Therefore, since every element of the vortex sheet has velocity  $(2\sigma_0 - a)U\epsilon/a$ , the vortex center of gravity at  $\sigma_0$  will possess that velocity.

Use of the Kutta condition at the leading edge, plus the force-free vortex system as the boundary condition, yields the solution of Ref. 4. If the Kutta condition is relinquished and the vertical position of the vortex is fixed at  $\frac{a}{4} \frac{a}{\epsilon}$ , the resultant solution of vortex position and strength is of the form shown in Fig. 19. The vortex starts at the wing centerline and moves slowly outboard with increasing  $a/\epsilon$ . No real solutions exist outboard of the 1/3 semi-span point. The vortex strength  $k/2\pi Ua\epsilon$  starting at zero is initially negative; it then reverses and takes on large positive values. The behavior of both  $y_0/a$  and  $k/2\pi Ua\epsilon$  is contrary to the observed physical flow and is considered to be the result of a basic inconsistency in the boundary conditions description of the flow at the leading edge.

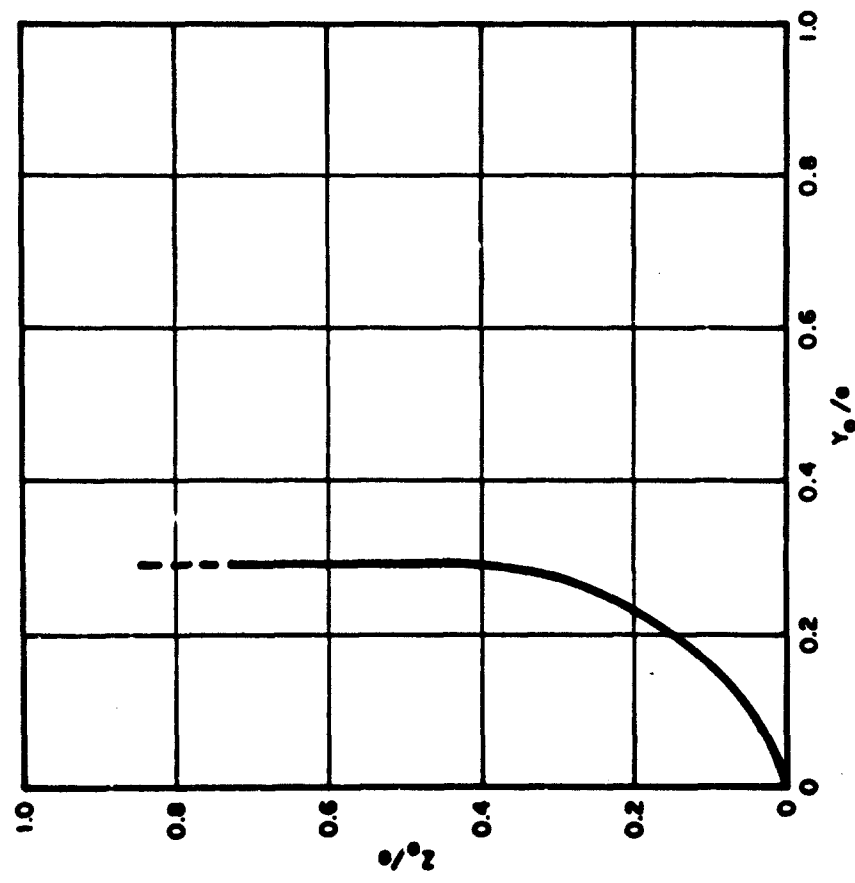
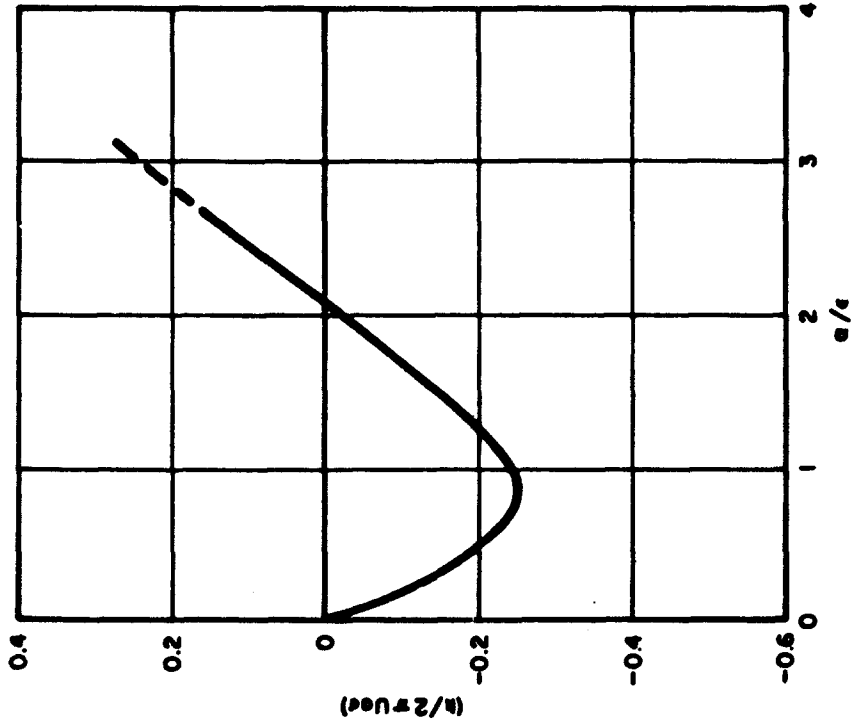


Figure 19. Force-Free Vortex Position and Strength.

## REFERENCES

1. W. J. Michael, Flow Studies on Flat-Plane Delta Wings at Supersonic Speed, Report TN 3472, NACA (July 1955).
2. Torsten Ornberg, A Note on the Flow Around Delta Wings, Report TN 38, KTH Aero (Sweden) (February 1954).
3. R. Legendre, "Ecoulement au voisinage de la pointe avant d'une aile a forte fleche aux incidences moyennes," La Recherche Aeronautique Bulletin Bimestriel, de l'Office National d'Etudes et de Recherches Aeronautiques (November-December 1952).
4. C. Brown and W. Michael, Jr., On Slender Delta Wings with Leading-Edge Separation, Report TN 3430, NACA (April 1955).
5. K. W. Mangler and J. H. B. Smith, Calculation of the Flow Past Slender Delta Wings with Leading-Edge Separation, Report Aero 2593, RAE (May 1957).
6. R. H. Edwards, "Leading-Edge Separation from Delta Wings," Journal of the Aeronautical Sciences (Readers' Forum) 21 (2) (February 1954) pp 134-135.
7. Mac C. Adams, "Leading-Edge Separation From Delta Wings at Supersonic Speeds," Journal of the Aeronautical Sciences (Readers' Forum) 21 (6) (June 1953) pp 430.
8. N. Rott, "Diffraction of a Weak Shock with Vortex Generation," Journal of Fluid Mechanics, 1 (Part 1) (May 1956).
9. R. T. Jones, Properties of Low-Aspect-Ratio Pointed Wings at Speeds Below and Above the Speed of Sound, Report TR 835, NACA (1946).
10. W. Bollay, "A Non-Linear Wing Theory and its Application to Rectangular Wings of Small Aspect Ratio," ZAMM Bd. 19 (1) (February 1939) pp 21-35.
11. K. Gersten, "Nichtlineare Tragflachen theorie, insbesondere fur Tragflugel mit kleinem seitenverhaltnis," Habilitationsschrift T. H. Braun Schweig 1960: Ingenieur-Archiv., 31 (11.6) (1961) pp 431-452.
12. H. R. Lawrence, The Lift Distribution on Low-Aspect-Ratio Wings at Subsonic Speeds, IAS Preprint No. 313 (January 1951).

## REFERENCES (Continued)

13. P. R. Fink and J. Taylor, Some Low Speed Experiments with 20° Delta Wings, Report ARC 17-854, Imperial College (September 1955).
14. R. W. May, Jr. and J. G. Hawes, Low-Speed Pressure-Distribution and Flow Investigation for a Large Pitch and Yaw Range of Three Low-Aspect-Ratio Pointed Wings Having Leading-Edge Swept Back 60° and Bi-convex Sections, Report TM L9J07, NACA (November 1949).
15. G. H. Lee, Note on the Flow Around Delta Wings with Sharp Leading Edges, ARC R and M No. 3070 (1958).
16. A. J. Bergeson and J. D. Porter, An Investigation of the Flow Around Slender Delta Wings with Leading-Edge Separation, Report No. 510, Princeton University, Department of Engineering (May 1960).
17. G. Drougge and P. O. Larson, Pressure Measurements and Flow Investigation on Delta Wings at Supersonic Speed, Report 57, FFA (Sweden) (November 1956).
18. G. H. Lee, Reduction of Lift-Dependent Drag with Separated Flow, ARC C. P. No. 593 (October 1959).
19. H. Winter, Flow Phenomena on Plates and Airfoils of Short Span, Report TM 798, NACA (1936).
20. Louis P. Tosti, Low-Speed Static Stability and Damping-in Roll Characteristics for Some Swept and Unswept Low-Aspect-Ratio Wings, Report TN 1468, NACA (1947).
21. G. E. Bartlett and R. J. Vidal, "Experimental Investigation of Influence of Edge Shape on the Aerodynamic Characteristics of Low Aspect Ratio Wings at Low Speeds," Journal of the Aeronautical Sciences, 22 (8) (August 1955) pp 517-533.
22. J. N. Nielson, E. D. Katzen, and K. K. Tang, Lift and Pitching-Moment Interference Between a Pointed Cylindrical Body and Triangular Wings of Various Aspect Ratios at Mach Numbers of 1.50 and 2.02, Report TN 3795, NACA (December 1956).

## REFERENCES (Continued)

23. S. Lampert, Aerodynamic Force Characteristics of Delta Wings at Supersonic Speeds, Report 20-82, Jet Propulsion Laboratory (September 1954).
24. R. L. Maltby and R. F. A. Keating, Flow Visualization in Low-Speed Wind Tunnels, Report Aero-2715, RAE (August 1960).
25. L. C. Squire, The Characteristics of Some Slender Cambered Gothic Wings at Mach Numbers from 0.4 to 2.0, Report Aero-2663, RAE (May 1962).
26. S. F. Hoerner, Fluid-Dynamic Drag (1958)

**BLANK PAGE**

## EXTERNAL DISTRIBUTION

Defense Documentation Center (20)  
Cameron Station  
Alexandria, Virginia

SSD (SSTRT) (2)

SSD (SSTRS)

AFCL (ERD Library)  
AFCL (CRRB)  
L. G. Hanscom Field  
Bedford, Massachusetts

AFFDL (FDS) (3)

AFAPL (APS)

AFML (MAS)

AFAL (AVS)

AFIT (Library)

SEG

Wright-Patterson AFB, Ohio

AFRPL (RPS)

Edwards AFB, California

RADC (EMS)

Griffiss AFB, New York

AFWL (WLS)

Kirtland AFB, New Mexico

AFOSR

Bldg T-D

Washington 25, D. C.

USNRL (Library)

Washington 25, D. C.

NASA Langley Research Center  
(Library)

Hampton, Virginia

Dr. Paul D. Arthur  
11221 Gloria Avenue  
Granada Hills, California

Dr. R. H. Edwards  
University of Southern California

Peter Lissaman  
California Institute of Technology

F. S. Malvestuto  
16775 Knollwood Drive  
Granada Hills, California

Dr. L. Schmidt  
c/o Aeronautics Department  
U. S. Naval Postgraduate School  
Monterey, California

D. Seager  
Lockheed Aircraft Company  
Burbank, California

T. Strand  
1065 Sorrento  
Point Loma, California

R. Skulsky  
United Aircraft Corporation  
1650 South Pacific Coast Highway  
Redondo Beach, California

NASA Lewis Research Center  
(Library)  
Cleveland 35, Ohio

NASA Ames Research Center (Library)  
Moffett Field, California

NASA Marshall Space Flight Center  
(Library)  
Huntsville, Alabama

## INTERNAL DISTRIBUTION

S. T. Chu  
G. E. Hlavka  
E. Levinsky (SBO)  
W. S. Lewellen  
C. A. Lindley  
J. G. Logan  
A. Mager  
A. E. Norem  
C. Pel  
B. Pershing (5)  
W. F. Radcliffe  
A. F. Robertson  
N. Rott  
W. P. Targoff  
N. R. O'Brien  
H. E. Wang